Impact of Pressure and Degradation on Morphology in Mesophase-Inducing Polymer Systems

By

Jelynn Tatad

Biochemistry and Molecular Biology, Sc.B, Brown University, 2024

Thesis

Submitted in partial fulfillment of the requirements for the Degree of Master of Science in the Graduate Program of Biotechnology at Brown University

PROVIDENCE, RHODE ISLAND

MAY 2025

AUTHORIZATION TO LEND AND REPRODUCE THE THESIS

As the sole author of this thesis, I authorize Brown University to lend it to other institutions for the purpose of scholarly research.

Date 4/30/2025 

Jelynn Tatad, Author

I further authorize Brown University to reproduce this thesis by photocopying or other means, in total or in part, at the request of other institutions or individuals for the purpose of scholarly research.

Date 4/30/2025 

Jelynn Tatad, Author

This thesis by Jelynn Tatad is accepted in its present form by the Graduate Program in Biotechnology as satisfying the thesis requirements for the degree of Master of Science

Date 4/23/25 Signature: Edith Mathiowitz

Dr. Edith Mathiowitz, Advisor

Date 4/23/25 Signature:

Dr. Benjamin McDonald, Reader

Date 4/23/25 Signature: Anita Shukla

Dr. Anita Shukla, Reader

Approved by the Graduate Council

Date _____ Signature: _____

Dr. Thomas Lewis, Dean of the Graduate School

Acknowledgments

I am incredibly proud to have been mentored by Dr. Edith Mathiowitz these past four years. She has encouraged me in all of my experiments, eased my anxieties about my research, and overall inspired me to pursue a career where I can remain passionate about science. She's been the best mentor throughout my undergraduate and master's years, and I'll miss her terribly as I move on from Brown University.

Additionally, I'd like to thank my committee members, Dr. Anita Shukla and Dr. Benjamin McDonald, for their time and willingness to help me with my thesis. Your expertise in your work has motivated me to become a better scientist. A special thanks goes to Timea Kolozsvary and the McDonald Lab for running my samples with their GPC equipment and helping me to understand the results I'm receiving. Another huge thanks to Dr. Hector Garces for his help with XRD these past three years. I've spent hundreds of hours in this room and you've always been such a supportive resource.

I'd also like to thank the many labmates I've interfaced with in my long tenure in the lab. The biggest thanks go to the friends who have made this lab a home for me: David Shafiei, Susan George, Floor Keuning, and Yashvi Deokule. Your friendship has kept me sane and happy during long work days, and I wish you all the best :)

I'd also like to thank the peers who have trained me and helped me with my experiments: Dr. Cameron Baptista, El Hadji Arona Mbaye, Raj Sharan, Anyaa Shah, Kosta Milovanovic, Apoorva Nagaraj Rao, Jingge Chen, Jacob Koster, Rudra Trivedi, and Zakhar Lyakovych. I'm extremely thankful for the guidance they've provided me in my time in the lab, and I'm honored to be able to continue some of the research that they've put forth in the lab.

Thank you to “my undergrads,” Logan Suryamega and David Veloso, for their friendship outside of our lab and for eagerly joining the lab this year.

Finally, I’d like to thank the rest of the lab and lab alums for their support: Vera Fonseca, Anthony Comeau, Zihao (Henry) Chen, Jiaying Yan, Gayathri Sundaresan, Ishitaa Gupta, William Borges, Tuyetanh Le, Hena Haque, Guanlin (Wilson) Wang, Michael DeSantis, Scott La Tour, and Liston Dsouza.

I’d like to especially thank my parents and my siblings, Jewelle and Jessela, for always encouraging me to follow my dreams, leading me to the world of science. Thank my partner Venkatsai Bellala for his constant support and willingness to listen to a rant about polymers. Finally, a huge thank you to Coco, Phoebe, and Emily Maranjian for their generosity in allowing me to live with them this year :)

Of course, I’d like to thank my friends for being my home away from home at Brown, from those who’ve supported my research journey to those who have supported me as a person. Without all of you, I would not be able to make it this far into my academic/research career.

Table of Contents

Table of Figures

Abstract of Impact of Pressure and Degradation on Morphology in Mesophase-Inducing Polymer Systems, by Jelynn Tatad, ScM, Brown University, May 2025.

Understanding polymer morphology is crucial in innovating new technologies for medical devices. This study focuses on characterizing how polymer blending influences morphology and how these morphological changes affect degradation behavior. Through the characterization of Poly-L-Lactic Acid (PLA), Polycaprolactone (PCL), and Polyethylene Oxide (PEO), key structural changes have been noted through Polarized Light Microscopy, where increased birefringence can be seen in processed samples, thereby suggesting increased order. XRD analysis quantified phase content, revealing that higher PLA content correlates with increased mesophase content. The results also showed that PEO/PCL blends maintain a high crystallinity and minimal mesophase formation. The PLGA degradation study demonstrated the impact of polymer morphology on degradation kinetics. GPC analysis showed that film-cast samples degrade the slowest, followed by mesophase-induced samples, and then unprocessed samples. A second degradation study involving PCL containing hydrophobic drugs (Dolutegravir and Meloxicam) showed the effects of processing temperature on polymer morphology and degradation rate. Minimal morphological changes and degradation were observed over the 3 month period, likely due to PCL's slow degradation rate. These findings confirm that increased order through mesophase induction indeed slows degradation, highlighting the link between morphology and degradation. This research provides key insights that are crucial in understanding future polymer applications within the biomedical device landscape.

Chapter 1: Introduction

Polymers

Polymers are an important hallmark of material science research due to their versatility[1] and cost-effectiveness in manufacturing[2]. With countless polymers in existence, the number of applications for these materials is endless. Biotechnology has found many uses for polymers in its various innovations within the field. Some examples of these uses are vascular grafts[3], tissue scaffolds[4], and bone fixators[5]. An application we will be focusing on is drug delivery. Polymers like PLGA have been used extensively for the delivery of drugs and proteins, while polyanhydrides have been used for injectable and oral deliveries.

Polymers are compounds that are made of smaller molecules known as monomers that repeat to create long chains. These chains can have vastly different properties depending on the chemical formula of their respective monomer[6]. A key characteristic of polymers is their morphology, which refers to the microscopic arrangement of the molecular structure.

Morphology is commonly classified by two main phases: amorphous and crystalline phases. The amorphous phase has a disordered structure, where the polymer chains are randomly arranged. These regions have a glass transition temperature, a point where the polymer shifts from a solid glassy state with limited motion, to a fluid rubbery state with rapid molecular motion[7].

The crystalline state has an ordered structure, which means the polymers are arranged in a lattice formation. These crystals can manifest themselves as spherulites, which are crystals that form radially. These structures contain an optical property known as birefringence, a

phenomenon referencing the refraction of light in two different directions due to a material's structure[8]. Due to its increased order, the crystalline phase degrades at a much slower rate than the amorphous phase[9]. While all polymers have an amorphous region, not all polymers have crystalline regions, as polymers cannot be fully crystalline. Crystalline regions have a melting temperature that is higher than the glass-transition temperature.

Previous work in our lab focuses on inducing an intermediate state known as mesophase into PCL[10] and PLA[11,12]. This phase is characterized by three different categories (nematic/liquid crystal, plastic crystal, and condis crystal) that are determined by their orientational, positional, and conformational order, where each mesophase has varying degrees of order[12]. In this paper, we will primarily be looking at the nematic mesophase and the condis crystal mesophases. Nematic mesophase has more order than the amorphous region, characterized by focused intensity in the middle of the XRD Debye rings though it remains diffused throughout the region. Condis crystal mesophase has less order than the crystalline region, where the Debye rings are more diffused although they maintain their positional order. A schematic showing the types of order each mesophase has can be seen in Figure 1. As an in-between region of the crystalline[6] and amorphous phases, inducing mesophase through means of time, pressure, and temperature allows for the polymer's morphology to be controlled.

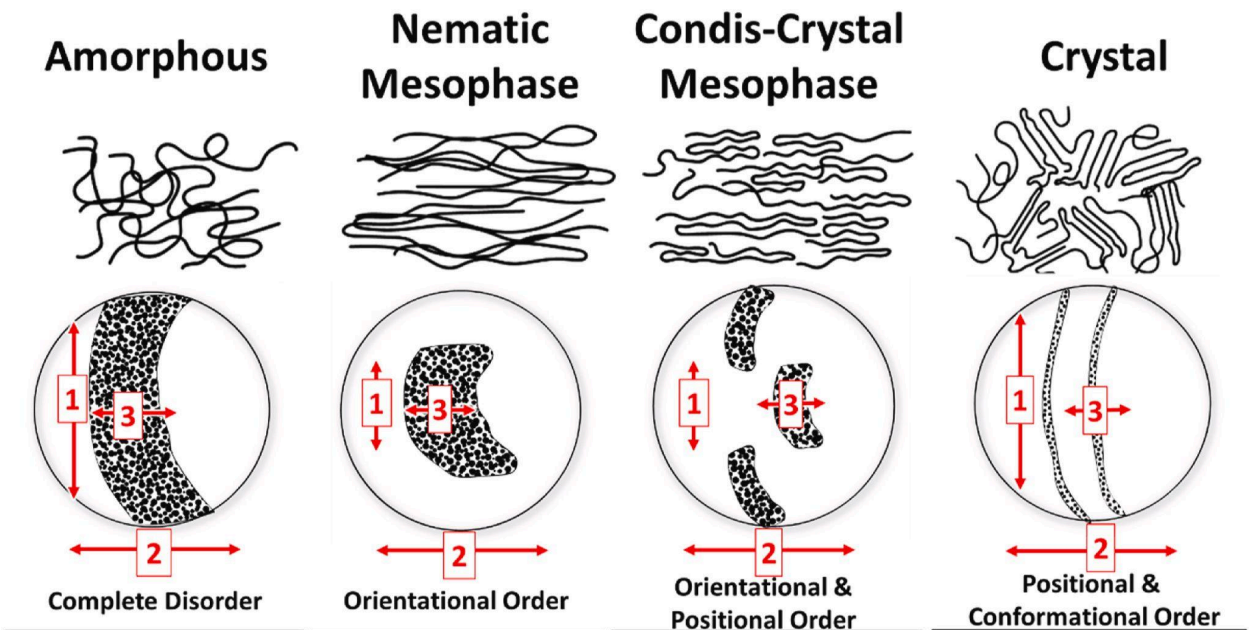

Figure 1: Schematic representation of polymer morphologies with their respective 2D-XRD azimuthal scattering patterns[12].

Polycaprolactone (PCL)

Polycaprolactone (PCL) is a synthetic polymer that has a semi-crystalline structure[13]. As a polyester created by polymerizing caprolactone rings[14], PCL is hydrophobic and has a glass transition temperature of -62ºC[15] and a melting temperature of about 60ºC. It is biodegradable and nontoxic[16], making it an ideal material for biomedical applications, being used in tissue engineering[17], dermal fillers[18], and bone scaffolds[19]. As a drug delivery vehicle, PCL has been formulated into hydrogels[20], nanoparticles[21], fibers[22], and scaffolds[23]. With a slow degradation rate[24], PCL has been popularly used for long-term drug delivery, typically blended with other polymers to control the degradation kinetics of the device[21].

Polyethylene Oxide (PEO)

Polyethylene Oxide (PEO) is a synthetic polymer with a semi-crystalline structure[25]. At a molecular weight below 20,000 g/mol, it is known as polyethylene glycol (PEG)[26]. Made of ethylene glycol monomers, PEO is hydrophilic and has a glass transition temperature of -50ºC[27] and a melting point of about 70ºC, depending on the molecular weight of the polymer[28]. With low toxicity, the polymer has been used in many drug delivery applications. Its water solubility has been utilized to make hydrophobic drugs more easily bioavailable in the body, through a modification known as PEGylation[29]. Other applications to drug delivery include oral tablets[30] and mucosal delivery matrices[31].

Poly-L-Lactic Acid (PLA)

Poly-L-Lactic Acid is a synthetic polymer with a semi-crystalline structure[32] that is derived from cornstarch but polymerized industrially. It is made from lactic acid monomers and has a glass transition temperature of 55-60ºC[33] and a melting point of 170ºC[34]. With its slow degradation rate, PLA has been commonly used for implants that need to be in the body for a long time[35]. Some examples of its use in the body are sutures[36], scaffolds to support gene therapy[37], synthetic bone flaps[38], and drug delivery of high molecular weight drugs[39].

Poly-lactic-co-glycolic acid (PLGA)

PLGA is a polymer synthesized from co-polymerizing PLA and polyglycolic acid (PGA). It is made from the hydrolysis of lactic acid and glycolic acid monomers[40], and its morphology is highly dependent on the ratio of the two polymers. At higher percentages of lactic acid monomers, PLGA is overall amorphous, whereas higher percentages of glycolic acid monomers make PLGA semicrystalline[41]. PLGA has a glass transition temperature of 40ºC[42] and does not

have a melting temperature at the ratios we will be looking at. PLGA is commonly used for drug delivery applications due to its biodegradability[43] and quick degradation rate.

Motivations

While the induction of mesophase in individual polymers continues be studied in our lab, there have yet to be studies on whether polymer blending can affect mesophase formation. PCL is a polymer commonly used for drug delivery purposes, and the blending of PCL with other polymers is hypothesized to affect its morphology. This can lead to more avenues for various drug delivery purposes, as polymers can be blended in various conditions to fit a pharmaceutical need. As such, our first aim of this project is to induce mesophase into implants with blended polymer composition and characterize their effects on the morphology when compared with samples created with only one polymer. This project also works on optimizing a deconvolution methodology for these samples that have blended composition.

In addition to polymer blending, the effects of mesophase on degradation behavior have not been extensively studied. Mesophase induction could be a valuable tool in modulating polymer stability, particularly when implanted in the body. In particular, we will be studying the degradation behavior of mesophase-induced PLGA, as PLGA's degradation behavior has been well-studied in many experiments. As PLGA is a primarily amorphous polymer, mesophase-induced PLGA is predicted to lead to a slower degradation rate compared to its unprocessed counterparts. This guides the second aim of this thesis.

Finally, we will be looking at the degradation behavior of PCL-drug implants. With PCL being a primarily crystalline polymer, it is expected to have a slow degradation rate, and given its

interactions with drug, we anticipate our polymer-drug implants having a slower degradation rate compared to pure PCL. This guides the third aim of the thesis.

To summarize, this project is guided by the following aims:

1. Characterize the morphology of PCL/PLA and PCL/PEO blends
2. Correlate processing conditions with Degradation Behavior in PLGA
3. Characterize the degradation of DTG-loaded and MLX-loaded PCL tablets

Chapter 2: Methods

2.1: Polymer Blend Characterization

2.1.1: Sample Fabrication

Samples were fabricated using three different polymers: poly(caprolactone) (MW: 37,000, Polysciences Inc.), poly(ethylene oxide) (MW: 100,000, Sigma-Aldrich), and poly(-L-lactic acid) (MW: 100,000, DURECT). Films contained 250 mg of two polymers blended at ratios of 25:75, 50:50, and 75:25, with polymer 1 being either PEO or PLA and polymer 2 being PCL. Pure samples of each polymer were also created as control samples to compare against the blended samples. This would create 9 different polymer compositions.

Processing Conditions							
Ratios	Temperature						Blends
	Film Cast	1st Press	25°C	40°C	55°C		
	100/0	100/0	100/0	100/0	100/0	PLA/PCL	
	75/25	75/25	75/25	75/25	75/25		
	50/50	50/50	50/50	50/50	50/50		
	25/75	25/75	25/75	25/75	25/75		
	100/0	100/0	100/0	100/0	100/0	PEO/PCL	
	75/25	75/25	75/25	75/25	75/25		
	50/50	50/50	50/50	50/50	50/50		
	25/75	25/75	25/75	25/75	25/75		
	100	100	100	100	100	PCL	

Figure 2: Table showing all samples that were fabricated with the conditions that were used

The polymer pellets are then dissolved in 2 mL of dichloromethane and subjected to a rigorous mixing process, which involves 3 rounds of sonication for 5 minutes and 1 minute of vortexing. After the polymers have been fully dissolved, the solution is poured into a 62 mm petri dish and left in a fume hood for 24 hours to allow the solvent to evaporate fully. This resulted in a thin film that can be peeled off the dish. For each polymer composition, one sample will remain as films for characterization purposes, to be referred to for the rest of the paper as "film-casts".

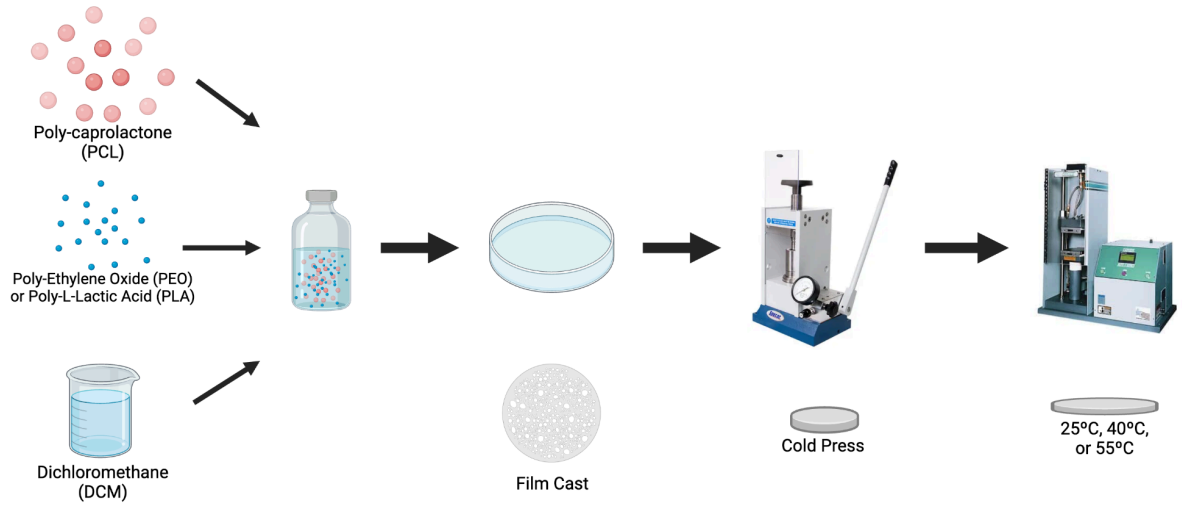

Figure 3: Schematic of Sample Fabrication Workflow.

Following the film casting process, samples are folded and placed into a 13 mm diameter cylindrical tablet die. The system is then pressed at 10,000 lbs at room temperature for 10 minutes in a Specac GS15011 manual hydraulic press. These will be known as the "first press" sample, and one sample per composition will remain in this form for characterization.

Next, these tablets are heat-pressed in a Carver Auto Press (Model 2889) between 2 steel plates and heated to either 25ºC, 40ºC, or 55ºC. This is followed by a 5-minute cooling period at 15,000 lbs that used a water and air-cooling system, with an end temperature of 25ºC. These samples will be referred to by their processing temperature in later analyses. This fabrication process is denoted in Figure 3.

This results in 45 samples from 9 polymer compositions and 5 different processing conditions, as denoted in Figure 2. Sample naming schemes are named for their percentage of polymer, Identity of polymer 1, and processing condition (for example: 25% PLA First Press, 100% PCL Film, 75% PEO 25ºC).

2.1.2: Polarized Light Microscopy (PLM)

Polarized Light Microscopy was performed using a Laxco SeBa Pro4B Series Digital Microscope System at 4x and 20x objectives. Images were captured using a 16MP Color Camera running on the SeBa Pro Software.

2.1.3: X-Ray Diffraction

X-Ray Diffraction is performed using a Bruker D-8 X-Ray Powder Diffraction machine. A Cu X-Ray tube is equipped and running at 40 kV and 40 mA with a Bruker Vantec-500 Xe-CO_2 gas-filled detector with a 13.5 cm diameter window located 20 cm from the goniometer center. Scans were run at a 2q angle from 20º to 80º with a 15º step size, with each step held for 30 seconds. Each scan produces a spectrum that shows the structural make-up of a material based on peak intensities at positions specific to the material being analyzed, as well as 2D-XRD images that show scattering patterns of the sample.

2.1.4: Peak Deconvolution Analysis

XRD spectra are quantified using a deconvolution methodology derived from protocols of Stoclet et al. and Galeski. This involves fitting Gaussian curves to fully evaluate the area underneath the curve, one broad curve spanning the primary area of interest and additional peaks that correspond to the unit cells into which the crystals of each polymer fall into according to literature. In PCL, these peaks are placed at 2θ values of approximately 21, 22, and 24. In PLA, these peaks will be placed at approximately 16, 19, and 22, and peaks at 19, 23, and 26 are used for quantifying PEO. Amorphous curves of processed samples (First Press, Heat Press) are derived from the film casts, and the amorphous region will be kept unchanged in our analysis. Wherever the crystalline peaks are unable to fill the area of the spectra, two mesophase peaks will be fitted to ensure a best fit analysis. Curves are adjusted to reach an r^2 value as close to 1.000 as possible, but with no less than an r^2 value of 0.975.

2.2: Degradation Studies

2.2.1: Sample Fabrication

2.2.1.1: PLGA degradation

Samples were created by weighing out 250 mg of poly(D, L lactide-co-glycolide) (viscocity: 0.67 dL/g, lactide: glycolide 75:25, BioPolymer Industries). The polymer pellets are then dissolved in 2 mL of dichloromethane and subjected to a rigorous mixing process, which involves 3 rounds of sonication for 5 minutes and 1 minute of vortexing. After the polymers have been fully dissolved, the solution is poured into a 62 mm petri dish and left in a fume hood for 24

hours to allow the solvent to evaporate completely. This resulted in a thin film that can be peeled off the dish. Some samples will remain as films for the degradation study.

Following the film-casting process, samples are folded and placed into a 13 mm diameter cylindrical tablet die. The system is then pressed at 10,000 lbs at room temperature for 10 minutes in a Specac GS15011 manual hydraulic press. Next, these tablets are heat-pressed in a Carver Auto Press (Model 2889) between 2 steel plates at 20,000 lbs and 50ºC for 10 minutes. This is followed by a 5-minute cooling period at 20,000 lbs that used a water and air-cooling system, with an end temperature of 25ºC. The samples are then removed from the press and stored away for characterization.

2.2.1.2: Degradation of DTG-loaded and MLX-loaded PCL tablets

PCL (CAPA 640, MW: 37 kg/mol, Perstorp Holding AB) was used as the vehicle for these tablets, with Dolutegravir or Meloxicam incorporated into the system. Films are created by weighing 225 mg of PCL and 25 mg of drug to create a system with a 10% drug loading. Samples without drug were also created as a control for this experiment. These films followed the film-casting protocol and first-pressed at 10,000 lbs at room temperature for 5 minutes. Finally, the tablets were heat-pressed at either 25ºC or 50ºC at 10,000 lbs for 10 minutes and cooled to room temperature.

2.2.2: Degradation Study

2.2.2.1: PLGA Degradation Study

A degradation study is conducted to characterize mesophase's effects on PLGA degradation. Samples are cut into 1 cm diameter disks, placed into scintillation vials with 10 mL

of 1X Phosphate-Buffered Saline (PBS), and placed into an incubator at 37 °C. The buffer is discarded and replenished every week that a sample is in the incubator. At specified time points (24h, 48h, 72h, 1W, 2W, 3W, 4W), the samples are washed twice in distilled water, lyophilized, and stored in a freezer until further analysis with X-Ray Diffraction. The solutions of the studies are subsequently discarded.

2.2.2.2: Degradation of DTG-loaded and MLX-loaded PCL tablets

Processed tablets are placed into falcon tubes containing 20 mL of PBS and incubated at 37ºC for the entirety of the study. Tablets were removed at specific time points (24h, 72h, 1W, 2W, 3W, 1M, 2M, 3M), and the solution was discarded. Tablets were lyophilized and then stored in a freezer until further analysis.

2.2.3: Polarized Light Microscopy (PLM)

Polarized Light Microscopy was performed using a Laxco SeBa Pro4B Series Digital Microscope System at 10x and 40x objectives. Images were captured using a 16MP Color Camera running on the SeBa Pro Software.

2.2.4: X-Ray Diffraction

X-Ray Diffraction is performed using a Bruker D-8 X-Ray Powder Diffraction machine to look at the polymer morphology of each sample before and after degradation. A Cu X-Ray tube is equipped and running at 40 kV and 40 mA with a Bruker Vantec-500 Xe-CO_2 gas-filled detector with a 13.5 cm diameter window located 20 cm from the goniometer center. Scans were run at a 2q angle from 20º to 80º with a 15º step size, with each step held for 30 seconds. Each scan produces a spectrum that shows the structural make-up of a material based on peak

intensities at positions specific to the material being analyzed, as well as 2D-XRD images that show scattering patterns of the sample.

2.2.5: Peak Deconvolution Analysis

XRD spectra are quantified using a deconvolution methodology derived from protocols of Stoclet et al. and Galeski. This involves fitting Gaussian curves to fully evaluate the area underneath the curve, one broad curve spanning the primary area of interest and additional peaks that correspond to the unit cells into which the crystals of each polymer fall into according to the literature. In PCL, these peaks are placed at 2θ values of approximately 21, 22, and 24. In PLGA, these peaks will be placed at approximately 16, 19, and 22, following the peaks found in PLA. Amorphous curves of processed samples (First Press, Heat Press) are derived from the film casts, and the amorphous region will be kept unchanged in our analysis. Wherever the crystalline peaks are unable to fill the area of the spectra, two mesophase peaks will be fitted to ensure a best fit analysis. Curves are adjusted to reach an r^2 value as close to 1.000 as possible, but with no less than an r^2 value of 0.975.

2.2.6: Size Exclusion Chromatography (SEC)

Size Exclusion Chromatography with Multi-Angle Light Scattering (SEC-MALS) was conducted on a TOSOH Bioscience EcoSEC Elite HLC-8420 GPC to calculate the molecular weight of degraded samples after each time point. Spectroscopic-grade tetrahydrofuran (THF) stabilized with 250 ppm butylated hydroxytoluene (BHT) was used at a flow rate of 0.7 mL/min with a 40 µL sample injection at 40ºC. The separation was performed on two TSKgel GMHhr-N columns in series, with an inner diameter of 7.8 mm, a length of 30 cm, and a mean particle size

of 5 μm. Refractive index increment (dn/dc) was measured with an integrated TOSOH Dual Flow RI detector and multi-angle light scattering (MALS) with a 20 ± 5 MW laser with a wavelength of λ = 505 nm at low (10º), right (90º) and high (170º) angles were connected in parallel with the RI. Data was processed in TOSOH SecView2.5 software.

Degradation study samples were analyzed with SEC-MALS by preparing a 1 mg/mL sample of the analyte in HPLC-grade THF with 1% BHT as the inhibitor and allowing solvation under gentle agitation for at least 12 hours. Samples were filtered through 0.2 μm filters before injection. A polystyrene (PS) standard with a narrow polydispersity (NIST 1478, 2.520 mg/mL, injection volume of 50 μL, Mw of 37,400 g/mol) was used for setting instrument parameters and instrument calibration. A dn/dc value of 0.185 mL/g was used for PS in THF. Column calibration was performed using 12 PS standards ranging from 1,110,000 Da to 589 Da with 3rd order fitting.

Chapter 3: Results and Discussion

3.1: Blended Polymer Characterization

3.1.1: PLM Images

The goal of analyzing samples using PLM is twofold: to gain insight into a polymer sample's structure and to note any changes between pure and blended samples. Images from the PLM are used to show the existence of birefringence and spherulites, thus providing a qualitative lens of the polymer structure. These are best shown in images of the film casts, where the spherulite formations can be seen (Figure 4). PCL (Figure 4A) shows spherulites interspersed with other regions, which can indicate phase separation. While PLA (Figure 4B) shows pronounced spherulites, PEO (Figure 4C) shows disrupted spherulites, possibly as a result of the solvent used in the film-casting step of preparation.

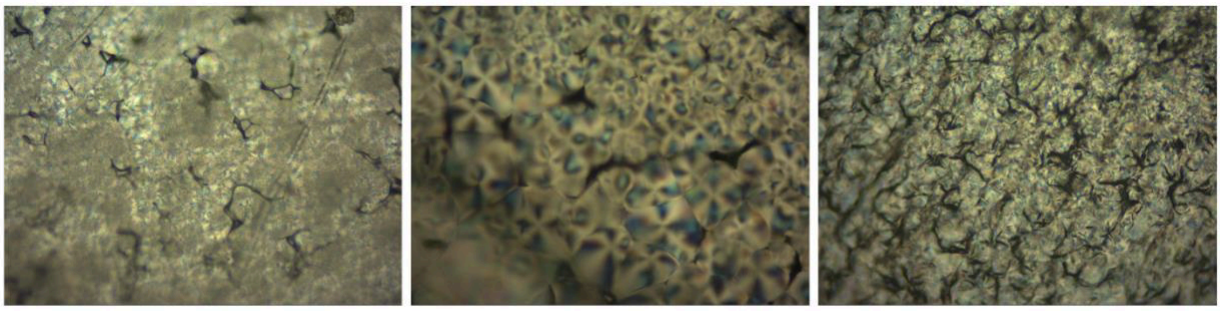

Figure 4: PLM images of unprocessed and unblended polymer films imaged at 20x magnification. (A) PCL. (B) PLA. (C) PEO.

The images in Figure 5 show blended PCL and PLA at the five different processing conditions. As the processed results are too thick to show pertinent details about the sample

morphology at the centers (Supplementary Figure 19), the images of the edges of the samples will be analyzed.

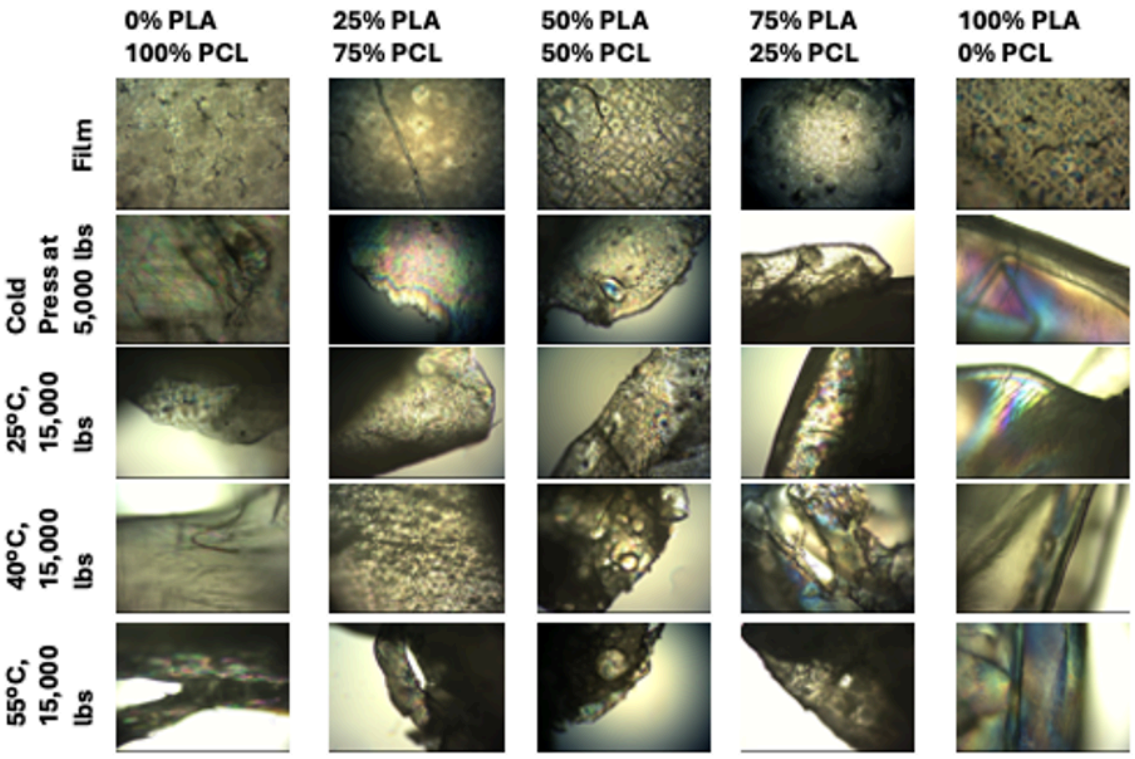

Figure 5: PLM images of PLA/PCL blends imaged edge of sample at 20x magnification.

Looking at the 100% PCL samples, spherulites are not visible, though birefringence is still present. This may indicate nematic mesophase formation, as orientational order is necessary for birefringence to be present. While the 25ºC and 55ºC samples show spherulites with birefringence, regions of birefringence without lamellar structures are present. The 40ºC sample yields similar results to the First Press sample, showing regions of birefringence without spherulites. Looking at the 100% PLA samples, there is a significant change in morphology with increased processing. While the film shows a strong presence of spherulites, none of the

processed samples show spherulites, though birefringence is present. Stronger birefringence can be seen in the first press and 25ºC samples, compared to the 40ºC and 55ºC samples.

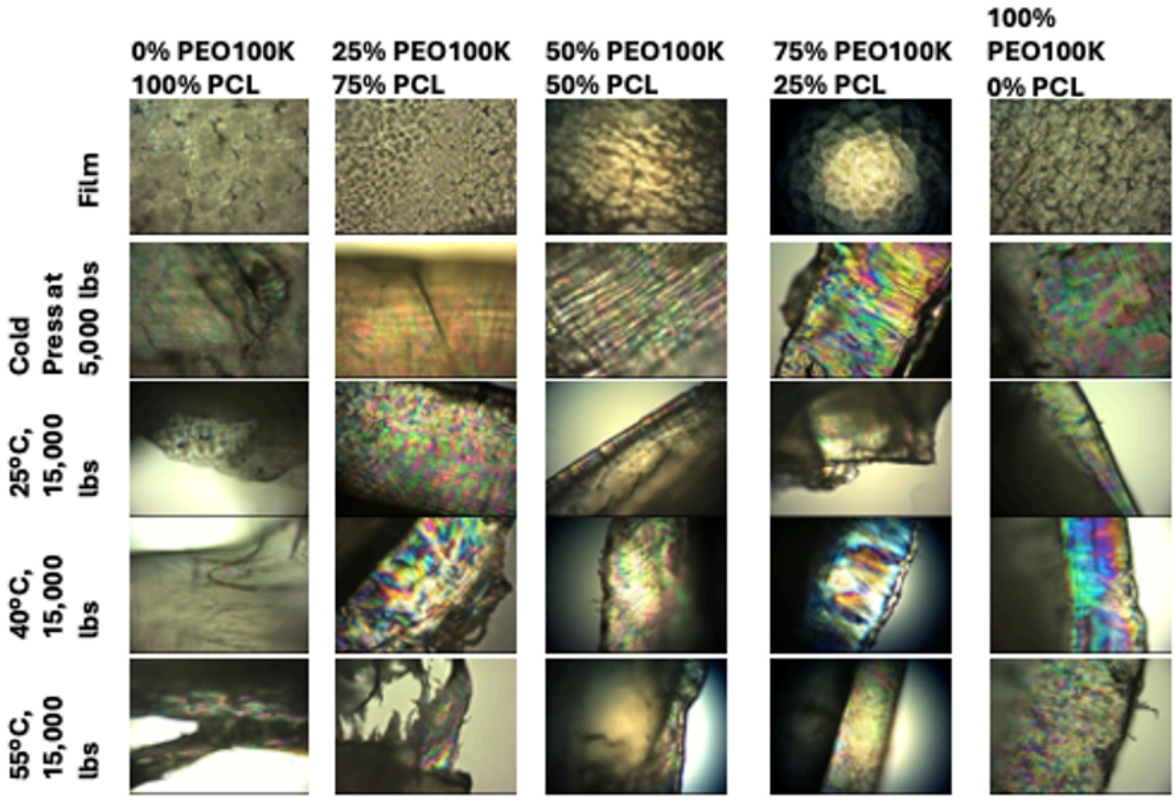

Figure 6: PLM images of PEO/PCL blends imaged edge of sample at 20x magnification.

In Figure 6, PEO shows very little birefringence as a film, though there is a strong presence of birefringence in the processed samples. The first press and 40ºC samples seem to show stronger birefringence compared to the 25ºC and 55ºC samples. It is also worth noting that there are no spherulites present in the processed samples, further suggesting morphological changes during pressure processing. Overall, PLM analysis of pure samples suggests the ability to induce morphological changes to a polymer compared to its unprocessed film form.

Additionally, changes between the blended and pure samples can be noted. In Figure 5, samples with higher PLA content show smaller regions of birefringence with few spherulites present. In contrast, unprocessed films of the 25% samples had larger spherulite formations that resembled the ones present in the 100% PCL Film. Meanwhile, the 50% samples had vastly different crystal formations than either of the pure PLA or PCL films. While large spherulites are present in pure samples, the 50% sample had much smaller structures. Some of the regions seem to have interrupted spherulite formation, potentially because of phase separation. The rest of the processed samples show spherulite formation, but in much smaller regions than what is seen in the pure samples. This is unlike the processed samples of the pure polymers, as no crystal formations were observed in these images. Processed samples with higher PLA content showed stronger birefringence. Despite the pure PLA sample having more well-defined spherulites, smaller crystal formations can be observed in the samples with higher PLA content. Based on this analysis, we can predict that samples with higher PLA composition might contain higher mesophase content due to the stronger presence of birefringence, whereas the samples with lower PLA content might likely have more crystalline morphologies.

Further looking at the PEO blends in Figure 6, spherulite formations are seen in nearly all of the films, with 75% PEO having larger structures, while the 25% PEO samples had smaller structures. Notably, the 50% PEO film does not show any spherulite formations, likely due to phase separation. This phenomenon occurs when two phases of a homogeneous solution separate and aggregate with their respective phase. In this case, PEO and PCL are separating into two distinct regions, possibly due to their immiscibility. PEO, being a hydrophilic polymer, would make it difficult to mix with the hydrophobic PCL, likely causing spherulite formation to be

disrupted under these conditions. In the processed samples, birefringence with a lack of lamellar structures is seen in nearly all samples, with a stronger birefringence noticed in the first press and 25ºC samples. This could indicate possible mesophase formation within the blended, processed samples. With increasing PEO content, the first press samples appear to have increasing levels of birefringence. The 55ºC samples appeared to have less birefringence than the other processed samples, likely due to the processing sample being close to both PEO and PCL's melting temperatures. Based on these observations, we can predict the first press and the 25ºC samples to have a larger mesophase content, while the 55ºC samples might have lower mesophase content.

The PLM images provide qualitative insight into a polymer's structure, using the presence of birefringence and spherulites to inform on what the phase content of the sample might be. To further confirm our predictions quantitatively, X-Ray Diffraction is needed to show the scattering patterns and percentage of each polymer phase of the samples.

3.1.2: 2D XRD analysis

XRD scans were completed for each sample, yielding scans showing the scattering patterns of each sample based on their structure. Thin Debye-Scherrer rings are characteristic of crystalline regions, while a halo-like effect in these scans represents the amorphous region. Referring to Figure 7, condis-crystal mesophase can be seen with slight broadening of the Debye-Scherrer rings, though uniform spacing can still be observed. Nematic mesophase can be seen when the rings have widened to a point where the spacing is no longer visible, though the intensity of the ring remains.

The scattering for the 100% PCL Film (Figure 7) shows 2 well-defined peaks that are seen within the frame. This is represented by the (110), (111), and (200) orthorhombic crystal peaks of PCL, which are located at 2θ values of approximately 21º, 22º, and 24º. As the rings located at the 21º and 22º are very close to one another, the two rings appear as one thick ring. Subsequently processed samples show broadening of their Debye-Scherrer rings. This may indicate the formation of the condis-crystal mesophase which is consistent with the PLM images showing birefringence with a lack of spherulites.

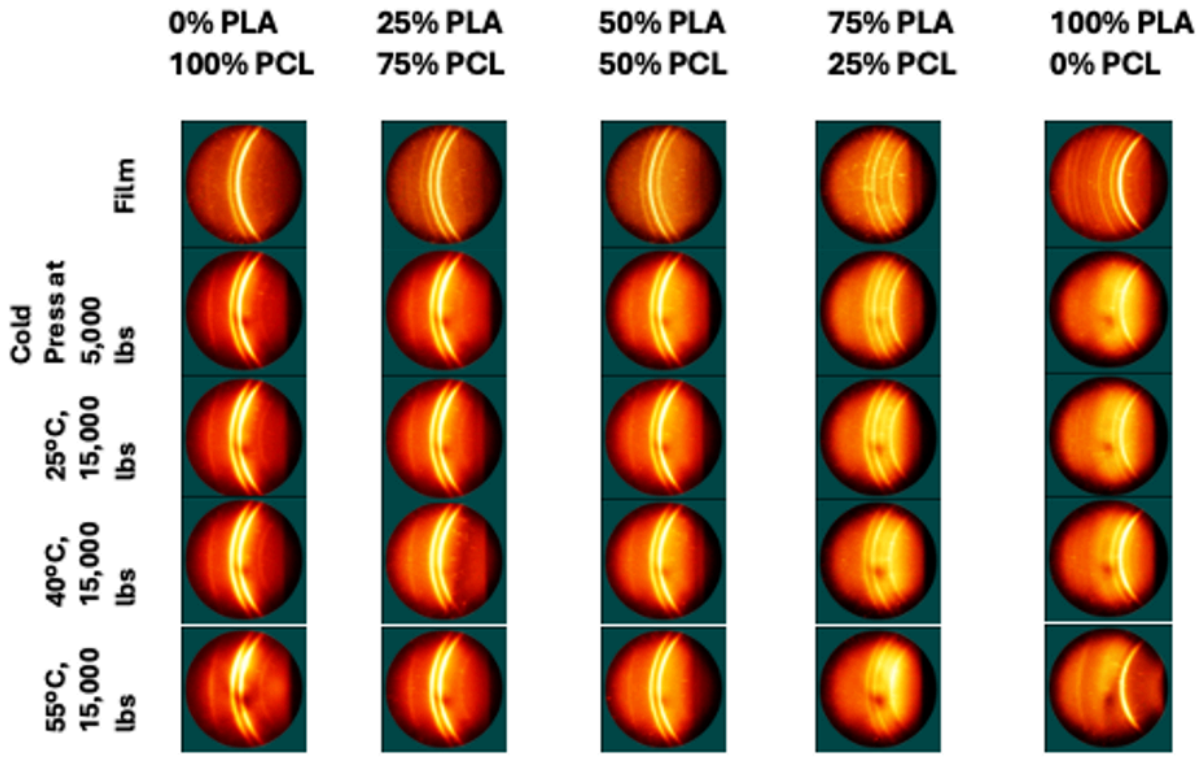

Figure 7: PLM images of PLA/PCL blends imaged edge of sample at 20x magnification.

The pure PLA film also shows a very crystalline sample, with orthorhombic crystallization face peaks at Miller Indices of (111) (200), (203), (015), which are located at 15º,

17º, and 22º, respectively. However, the processed samples show a prominent amorphous halo that nearly obscures the crystalline peaks that are present. This is characteristic of a nematic mesophase being induced.

When looking at the blended samples, it appears as though there are 4 rings present, though there are 6 primary peaks to take note of. These correspond with the crystalline peaks of their constituent polymers. With processing, these rings become broadened. At higher percentages of PLA, a much more prominent halo is observed in the films, indicating a potential induction of nematic mesophase. In samples with less than 50% PLA content, the crystalline rings maintain their same position, despite broadened scattering, indicating a condis-crystal mesophase. Comparing the blended samples to the pure samples, it appears that the 25% and 50% PLA samples appear most like pure PCL samples, while the 75% PLA samples are most similar to the pure PLA samples.

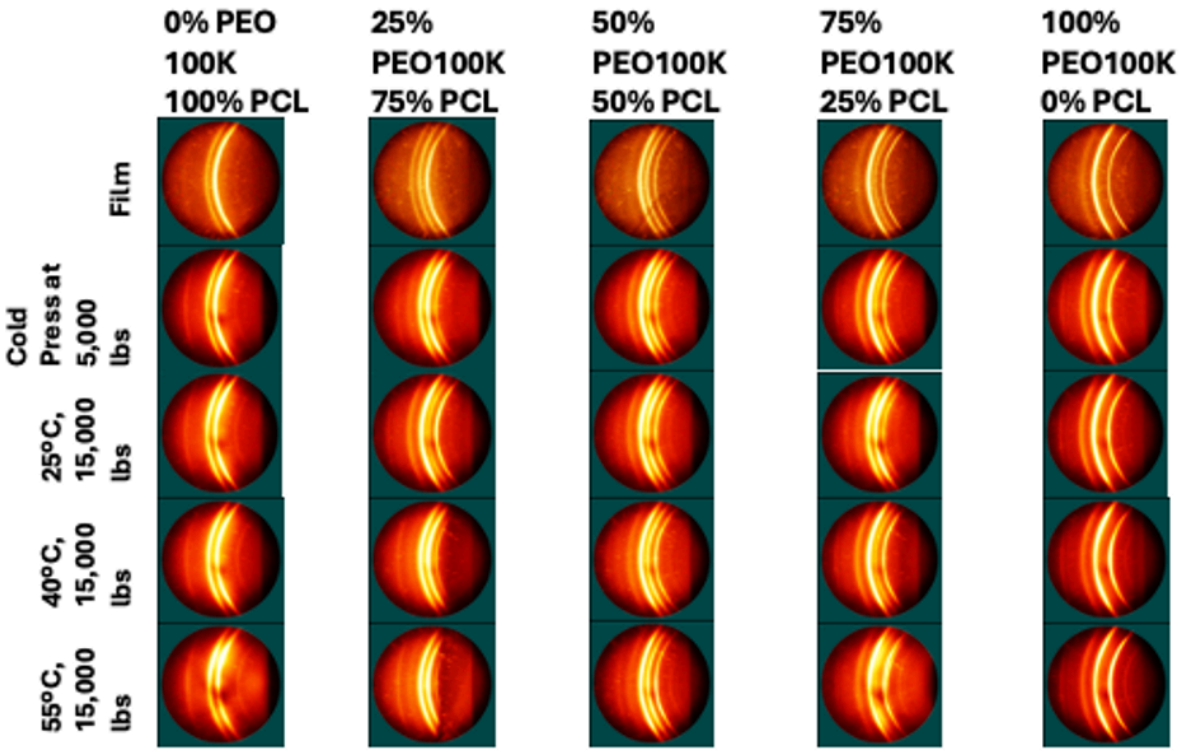

Figure 8: PLM images of PEO/PCL blends imaged edge of sample at 20x magnification.

In Figure 8, pure PEO is comprised of three main Debye-Scherrer rings in the (112), (120), and (222) monoclinic planes, which are located at approximately 19º, 23º, and 26º[44]. It is accompanied by a very faint halo, indicating little amorphous content. With increased processing, the rings undergo peak broadening without losing positional order, indicating condis-crystal mesophase. Within the blended samples, the six Debye rings corresponding to their respective polymers are present, having a strong presence in the samples that contain more than 50% PEO content. In processing, we start to notice the rings become less sharp, and a halo within the scan is more prominent. Since we are still able to distinguish the rings that correspond to each polymer but see more of a halo effect, we can propose that the type of mesophase we are

looking at is condis crystal mesophase. There doesn't appear to be any particular trend that we notice at different ratios of polymers.

3.1.3: Deconvolution XRD analysis

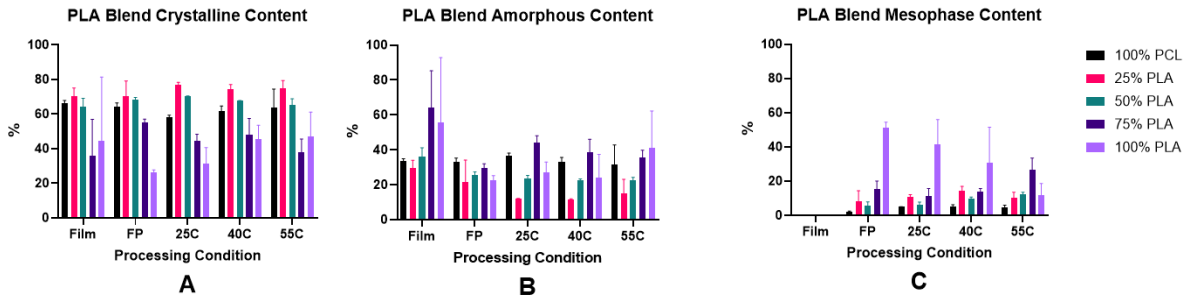

Figure 9: Phase content comparison of the PLA/PCL Blends. (A) Crystalline Content. (B) Amorphous Content (C) Mesophase Content.

Figure 9 shows an overview of the phase content calculated in peak deconvolution for the PLA/PCL blends. Looking at the crystalline content (Figure 4A) of the processed samples, crystallinity content remains similar compared to the films with some variation, except with pure PLA. A high standard deviation is seen with the pure PLA samples, which shows that the films are not homogeneous. This is expected, as PLA is a semi-crystalline polymer and will have some regions of high crystallinity and some of high amorphous content.

Looking at the amorphous content (Figure 9B), we see our highest amorphous content in the film casts, which makes sense as we are working with the assumption that our films only contain crystalline and amorphous regions. From then on, we start to notice an overall decrease in amorphous percentage with processing. This means that it's likely that most of the mesophase

content will come from the amorphous region, with some coming from the crystalline regions. Blended samples with less PLA content seem to have less amorphous content throughout.

Looking at the mesophase content (Figure 9C), increased processing leads to increased mesophase. Notably, the condition with the highest mesophase content is the pure PLA samples for all processing conditions, except for the 55ºC condition. A trend of increasing mesophase content is seen from the first press processing up to 40ºC, with a drop off at 55ºC. This trend is seen in all samples except 75% and 100% PLA.

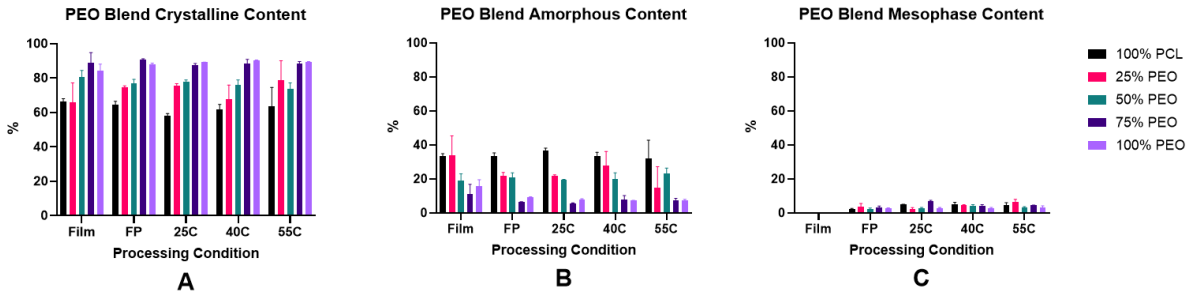

Figure 10: Phase content comparison of the PEO/PCL Blends. (A) Crystalline Content. (B) Amorphous Content (C) Mesophase Content.

The PEO/PCL blends show different trends. Looking at the crystallinity content (Figure 10A), the samples are very crystalline overall. Increasing the PEO content indicate higher crystallinity. Heat and pressure processing do not change the crystallinity content significantly in any of the PEO/PCL blends. Looking at the amorphous content (Figure 10B), the highest amorphous content can be seen in the pure PCL samples. The data also suggests that increasing PEO content decreases amorphous content.

Looking at the mesophase graphs (Figure 10C), we see that all of the samples have very low mesophase content. Though there is increasing mesophase content with increasing processing temperatures, the mesophase content remains throughout all polymer blends and processing conditions within the PEO/PCL blends.

3.2: PLGA Degradation Study

3.2.1: PLM Images

Though PLGA is typically an amorphous polymer, its constituent monomers that could result in crystalline phase depending on the copolymer and may still be observed in the sample as small spherulites. It would also be interesting to point out structural changes that occur throughout the degradation process.

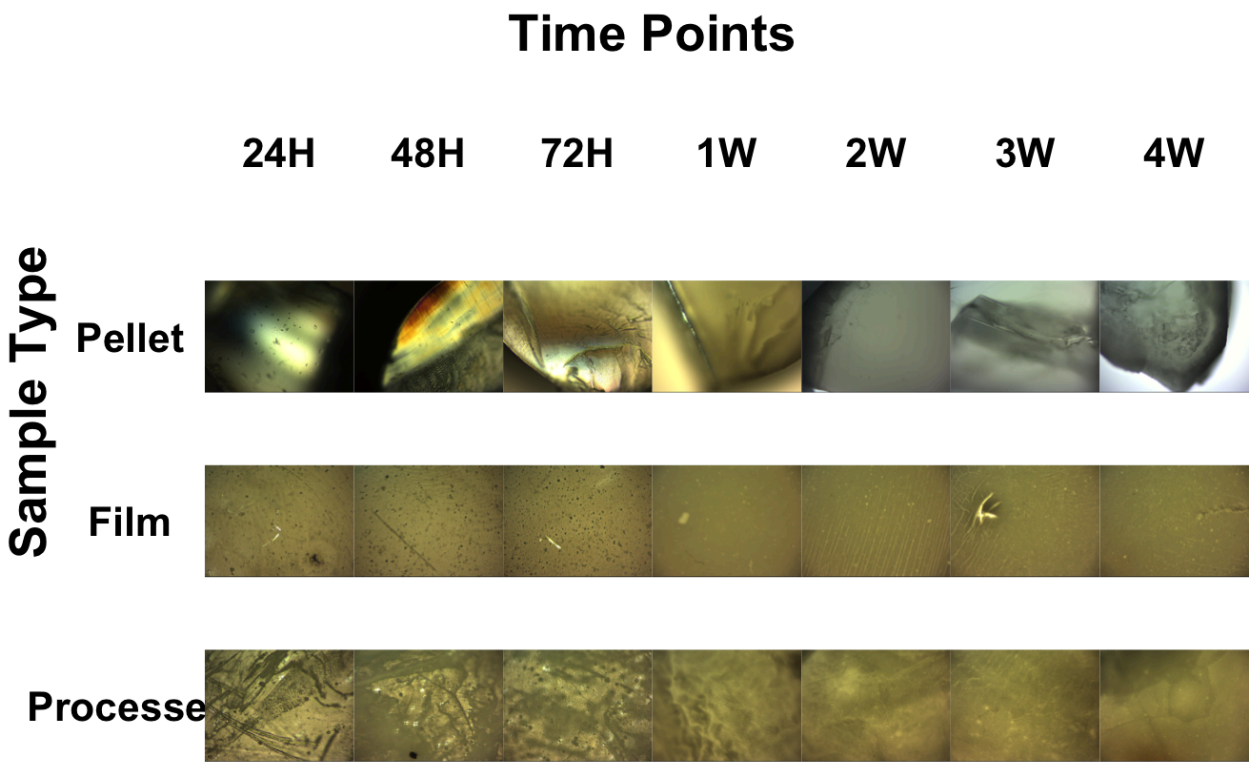

Figure 11: PLM images of degraded PLGA samples at 10x magnification.

Looking at the PLGA pellet images (Figure 11), crystal formations can be seen in the 24H and 48H samples. In the 24H sample, these manifest as small spherical structures, whereas the 48H crystals appear as a long branch of crystal. Interestingly, the 72H and 1W samples do not appear to have any crystal structures present, but birefringence is present. The pellets are assumed to be unprocessed samples without mesophase present, so the birefringence without crystal formation is interesting to take note of. This can be due to pre-processing of the pellets that may have been done before purchasing these samples, as the pellets are thought to have been extruded. This extrusion can potentially cause some type of morphological changes, which may have been reflected in the PLM images. Within the film samples, the 24H, 72H, and 3W samples seem to show a similar long crystal formation as the 48H pellet sample. This aligns with what we expect to see, as the film-cast samples are the most crystalline form of our polymer.

In the processed samples, spherulite formation can be seen in the 24H, 48H, and 72H samples. The most prominent presence of spherulites can be seen in the 48H sample, as these structures are present in the 10x magnification, whereas the 24H and 72H spherulites are only seen in the 40x magnification (Supplementary Figure 20). No birefringence is observed in these samples. The presence of spherulites could be a result of amorphous region being degraded first, revealing the presence of crystal structures.

3.2.2: Degradation Study Observations

The degradation study yielded interesting physical observations. Before the study, all samples were transparent, with the film and processed samples being punched out into 1 cm

diameter disks. After 24 hours, the shape of the processed samples morphed from a disk shape to a crescent moon-like shape. After 72 hours, the films and processed samples became opaque, possibly indicating morphological changes. The pellets became translucent after 1 week, and when cut in half, a transparent "core" remained on the inside. This transparent core would become smaller as the study progressed. In the 4W pellets, bubble-like formations were discovered on two of the samples, potentially indicating degradation or morphological changes.

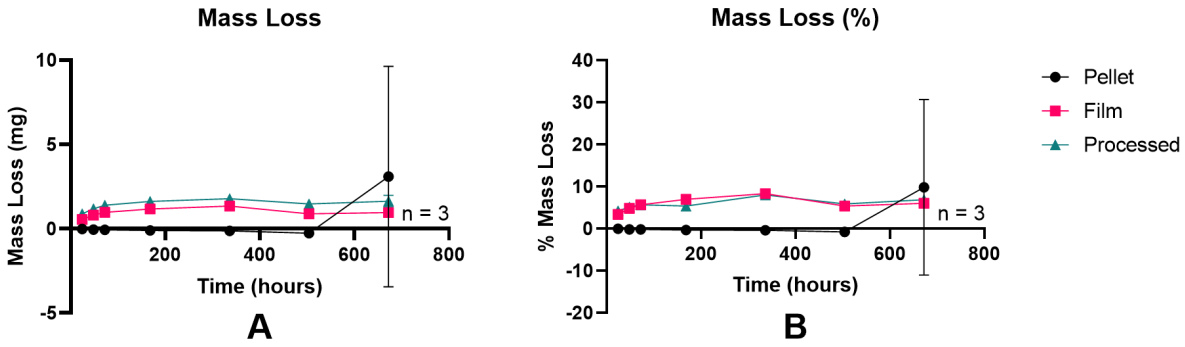

Figure 12: Graphs of PLGA mass loss during degradation study. (A) Mass loss in mg. (B) Mass loss in percentage.

Other interesting observations included the sample mass loss throughout the study. Though we would expect the samples to lose mass throughout the study, the pellets seemed to experience a gain of mass (Figure 12A) until the final timepoint at 4 weeks. This could be due to salts or degraded monomers remaining within the system. A drastic mass loss is observed at the 4-week time point, due to one of the samples breaking off a portion of its system in the lyophilization process. Though the processed samples experienced a higher mass loss compared to the films, they lost a similar percentage of mass throughout the study (Figure 12B).

3.2.3: GPC analysis

GPC allows us to gain insight on the molecular weight changes that occur during degradation of our samples. Analysis with this instrument produces information about a sample's molecular weight, allowing us to know how much of the sample has degraded at a given timepoint.

Due to the nature of polymer degradation, the polydispersity index (PDI) (Figure 13D) increases with longer degradation time. To encapsulate all of the polymer data at lower molecular weights, the GPC data integrates over a much longer range. This range also includes peaks that are known to correlate with the solvent peaks, a limitation of the instrument that is being used to analyze the data.

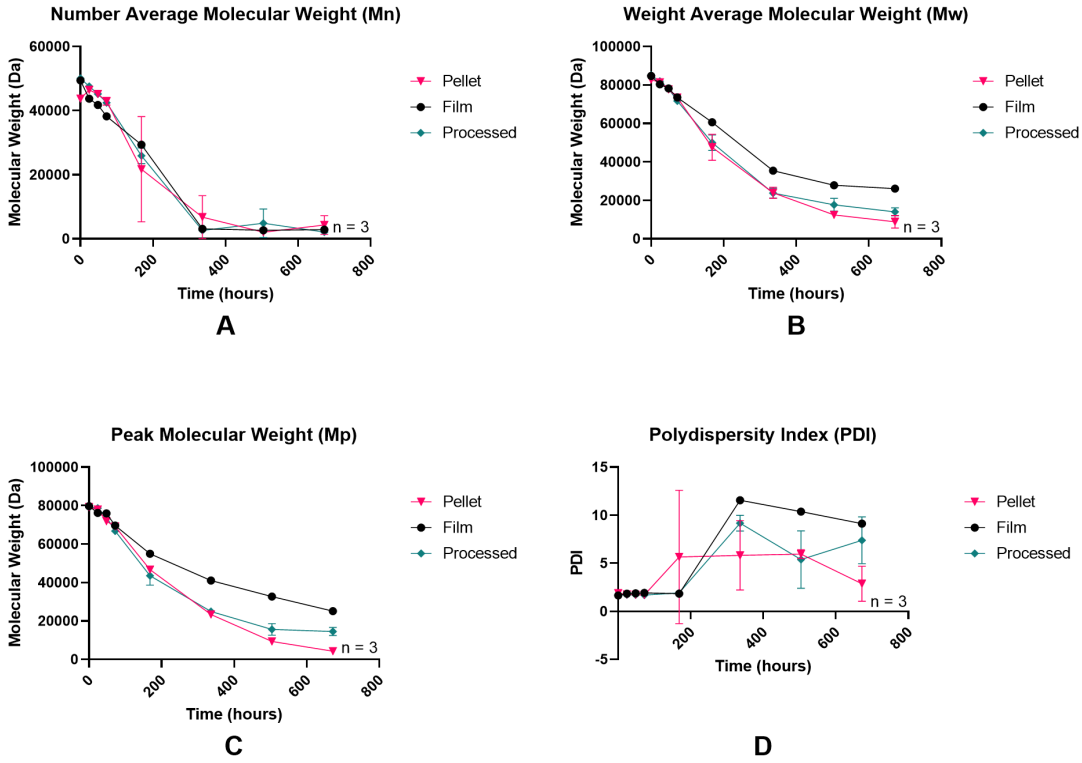

Figure 13: Molecular weight analysis graphs of degraded PLGA samples. (A) Number Average Molecular Weight (Mn). (B) Weight Average Molecular Weight (Mn). (C) Peak molecular Weight (Mp). (D) Polydispersity Index (PDI)

Looking at Mn (Figure 13A), degradation behavior appears to be similar in all three processing conditions. Molecular weight decreases slowly in the first 72 hours of degradation, with a significant decrease in Mn after the 2-week timepoint. Looking at Mw (Figure 13B), degradation behavior is similar for all three conditions for the first 72 hours. Beginning at the 1-week timepoint, the films begin to show significantly slower degradation compared to the pellet and processed samples. Similar trends can be seen with Mp (Figure 13C), which represents the mode of the weight distribution. By the end of the study, the pellets show faster degradation compared to the processed samples. This suggests that the films have the slowest degradation rate, followed by the processed tablets, and the fastest being the unprocessed pellets.

3.2.4: 2D-XRD Analysis

2D-XRD scans (Figure 14) were taken of the samples to further document morphological changes within the degraded samples overtime. Overall, the PLGA that we are experimenting with is mostly amorphous. The XRD frames do not show any easily-distinguishable Debye-rings, and all of the samples have a halo effect representing their amorphous regions. The amorphous halo in the pellet samples shows the least intensity, suggesting that the sample is very amorphous at this condition. This is expected, as the pellets have not been treated with time or pressure, so morphological changes are not expected at this point. This is interesting, as the PLM image of the 48 hour pellet (Figure 13) shows birefringence, which does not align with what we are seeing in our XRD for that sample.

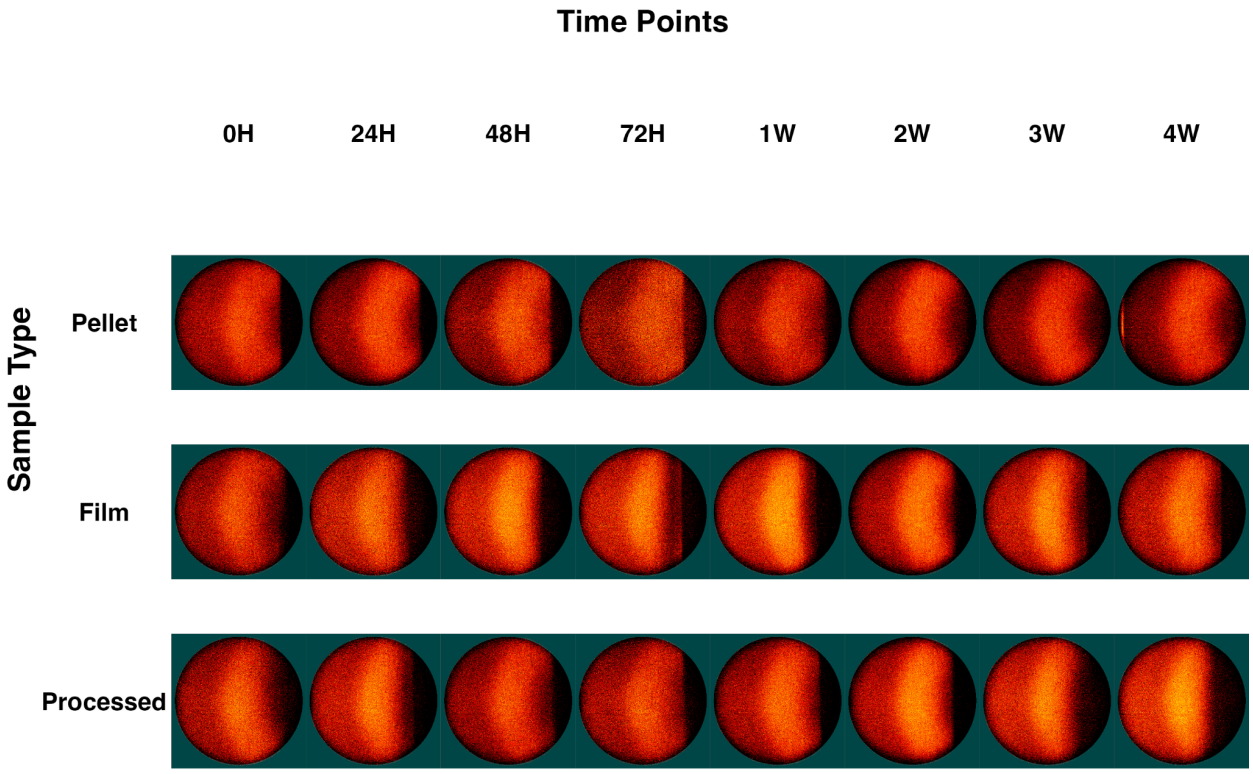

Figure 14: 2D-XRD scans of PLGA Degradation Study Samples.

The film samples have a halo with higher intensity, which suggests increased order within the polymer structure. As these samples also have not been treated with time nor pressure, we can predict that this is due to increased chain interaction due to the solvent-casting process. Higher intensity suggests that the films may have a higher crystalline content compared to the pellet samples. The processed samples do not display as much intensity as the film-casted samples, but have more than the unprocessed pellets. As these samples have been processed with time and pressure, this could suggest that mesophase formation has taken place.

3.3: Degradation of DTG-loaded and MLX-loaded PCL tablets

3.3.1: 2D-XRD Analysis

Looking at the samples processed at 25ºC (Figure 15), the samples without drug and the samples containing Dolutegravir show two prominent Debye rings that correspond to the (110) and (200) orthorhombic crystal peaks of PCL. Other minor rings can be seen in the MLX samples, which likely represent peaks that are present in Meloxicam. thin rings seen throughout with little amorphous halo, suggesting high crystallinity. Compared to the blank samples, more prominent halo effects can be seen in DTG and MLX samples. The second ring (which corresponds to the peak at 23º) is broader in the DTG and MLX compared to the blank sample, which can be an effect of polymer-drug interaction.

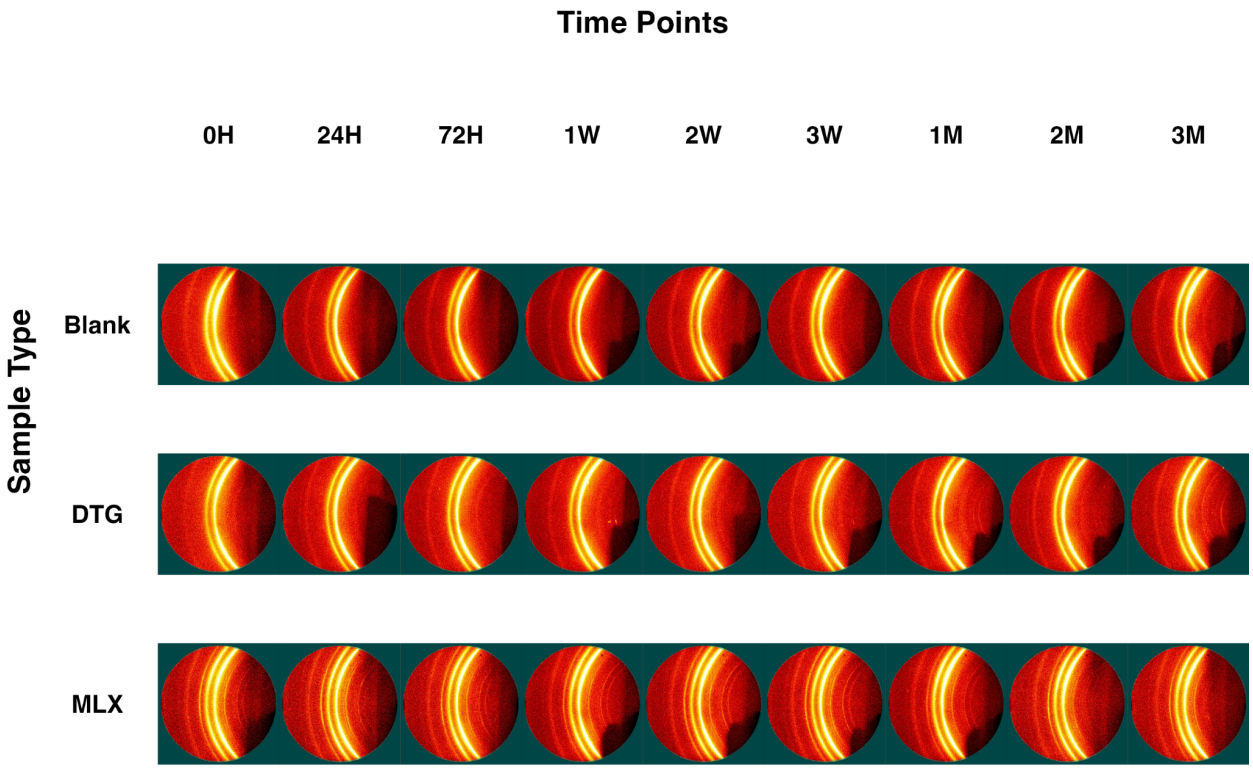

Figure 15: 2D-XRD images of polymer-drug samples processed at 25ºC after degradation timepoint.

Looking at the 50ºC samples (Figure 16), the additional Debye rings representing MLX are especially noticeable under 50ºC processing. Interestingly, the 3 Month MLX samples have rings that seem to have gotten thinner, contrary to the broadened rings that are seen in the other samples. there appears to be more ring broadening in comparison to the 25ºC samples. Despite this, there does not appear to be any peak broadening trends in relation to time. This can be further explained using deconvolution analysis of the XRD Scans.

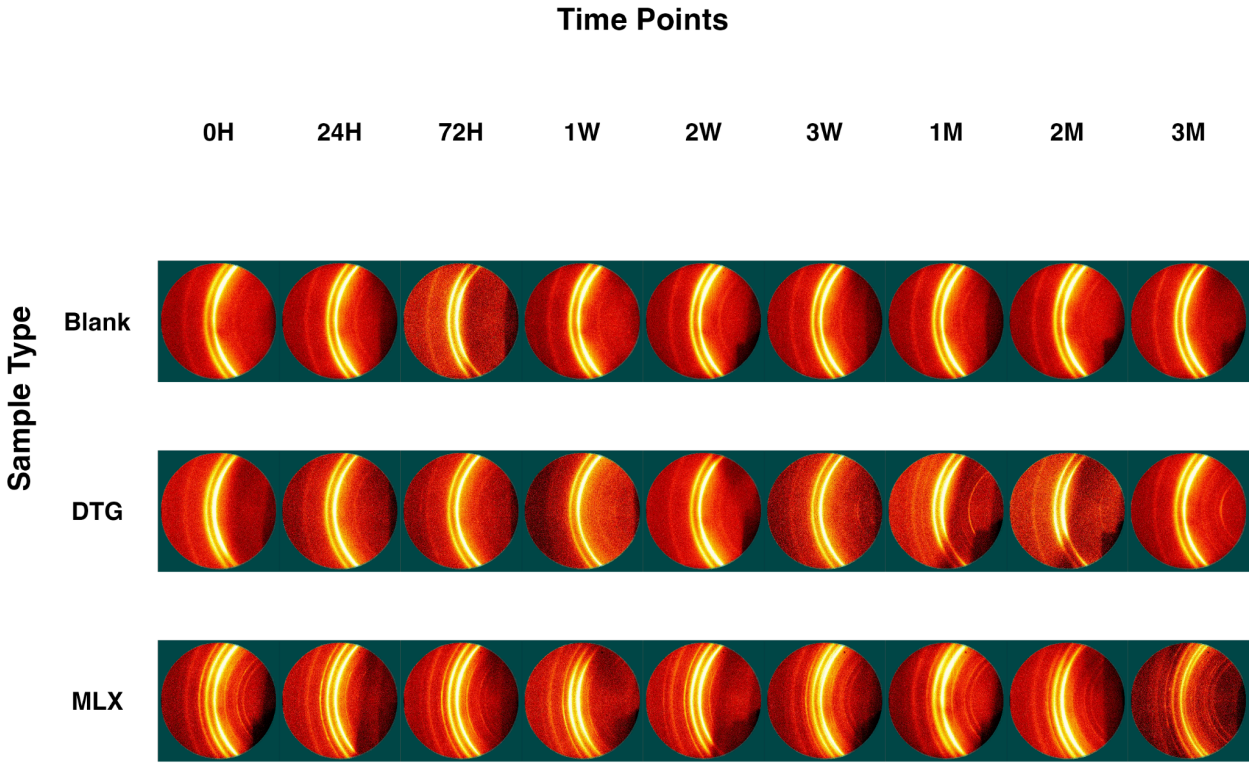

Figure 16: 2D-XRD images of polymer-drug samples processed at 50ºC after degradation timepoint.

3.3.2: Deconvolution Analysis

Deconvolution is done to study the effect of drug interactions with polymer morphology, as well as note any morphological changes throughout the 3 month degradation study. It should

be noted that the deconvolution of these samples only looked at the morphology of the PCL device, so the drug peaks were not included in the deconvolution calculations.

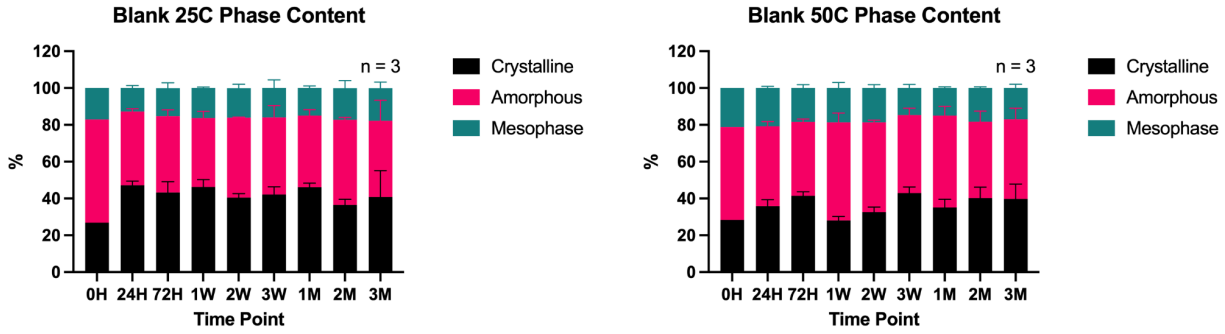

Figure 17: Deconvolution Comparisons of Blank Samples processed at 25ºC (left) and 50ºC (right).

First, we will look at the deconvolution results of the blank samples (Figure 17) that do not contain any drug. At both processing temps, samples contain the least crystalline content prior to degradation. While there are changes in crystalline and amorphous content between the processing temperatures and throughout the study, these changes are not found to be statistically significant. Mesophase content remains virtually the same throughout the study, regardless of time and processing temperature. Compared to the other samples, the blank samples tend to have the highest crystalline content over time. Despite this, results show that the samples are primarily amorphous, which doesn't align with the XRD scans we have.

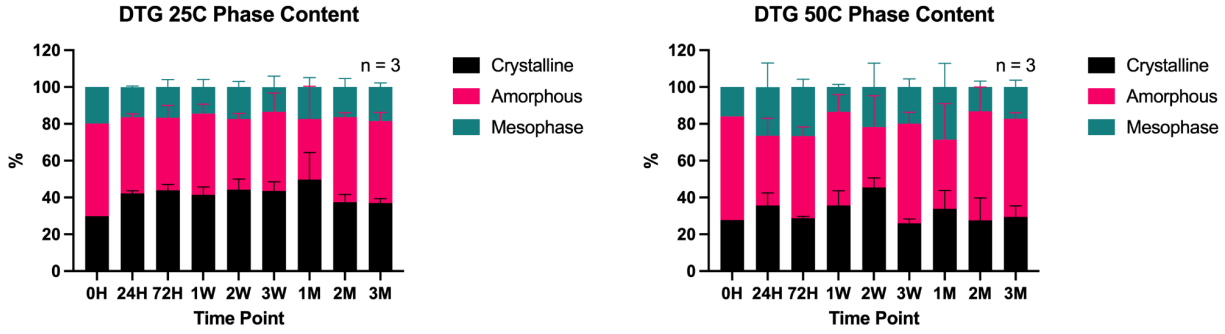

Figure 18: Deconvolution Comparisons of DTG Samples processed at 25ºC (left) and 50ºC (right).

Looking at the samples that contain DTG (Figure 18), mesophase content in 25ºC sample stays relatively similar throughout, while there is a lot more variance in the 50ºC samples. 50ºC samples see higher amorphous content in the samples that have been degraded for more than 1 month, compared to the 25ºC. There appears to be similar mesophase content in both the blank and DTG samples, with the DTG 25ºC samples having similar results to the blank samples. There does not appear to be any significant trends correlating phase content changes with degradation time or processing temperature within the DTG samples.

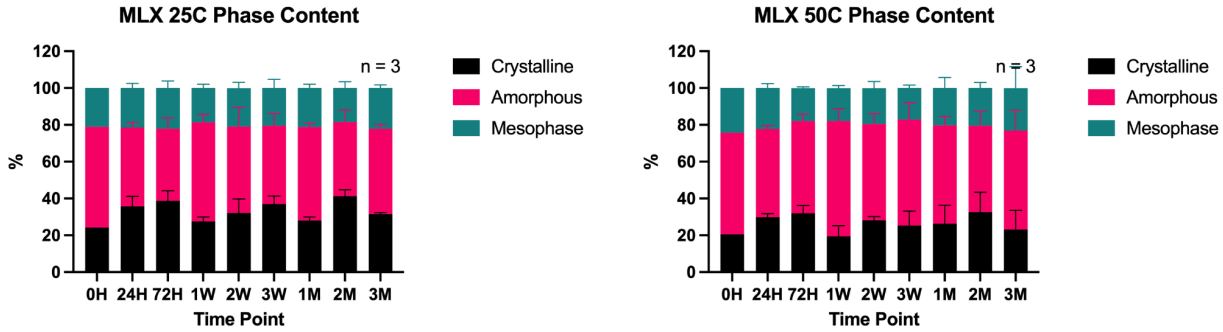

Figure 19: Deconvolution Comparisons of MLX Samples processed at 25ºC (left) and 50ºC (right).

Finally, we will look at the samples that contain MLX (Figure 19). Mesophase content remains relatively the same, regardless of processing temperatures and degradation time. The results show that the samples processed at 50ºC have low crystalline content. Additionally, there is also significantly higher amorphous content, compared to the blank and DTG samples. Overall, there are higher percentages of mesophase compared to the previously discussed samples. Once again, there does not appear to be any significant trends correlating phase content changes with degradation time or processing temperature within the MLX samples.

There are several possible explanations for the results that we are seeing with these PCL tablets. The primary reason is that polymers are naturally heterogeneous. Therefore, even analyzing different regions in the same sample may not express the same properties, as seen by the high SD in some of the results. Another reason could be that the samples did not degrade for long enough. PCL is a polymer with a slow degradation time, with research finding that the polymer takes 2-4 years to fully degrade[45]. A 3 month study may not be enough time for morphological changes to take place, therefore yielding results that are not statistically significant.

3.3.3: GPC analysis

GPC was run on the samples to observe any connection between polymer morphology and degradation rate. For this section, samples with the same composition will be compared against different processing temperatures.

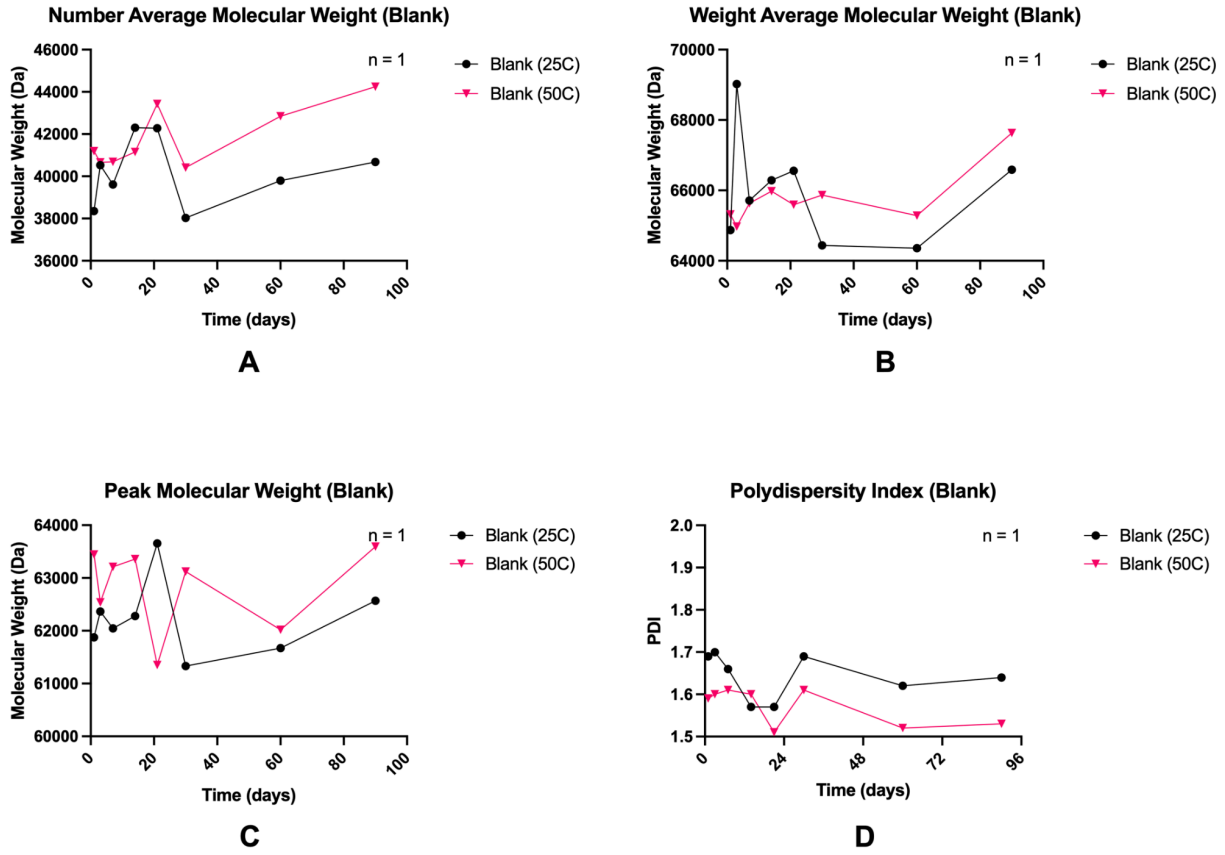

Figure 20: Molecular weight analysis graphs of PCL blank samples. (A) Number Average Molecular Weight (Mn). (B) Weight Average Molecular Weight (Mn). (C) Peak molecular Weight (Mp). (D) Polydispersity Index (PDI)

Figure 20 looks at the GPC results of the blank PCL samples. Looking at the Mn results (Figure 20A), the samples processed at 25ºC tended to have a lower Mn over time than the samples processed at 50ºC. Though we would not typically be expecting an increase in Mn after a 3 month period of degradation, it is worth noting that the samples may not have degraded enough to see significant decrease and the PCL pellets that were used for the 3 month samples may have had a higher actual Mn than those used in the samples that were removed after a shorter amount of time. Similar trends can be seen within Mp and PDI, where the values seen in

the 50ºC samples are greater than those of the 25ºC. In the Mw results (Figure 20B), the 25ºC samples start off by degrading slower than the 50ºC samples, but eventually observe lower Mw values after a month. Overall, these results suggest that PCL processed at 50ºC has a slower degradation rate than PCL processed at 25ºC.

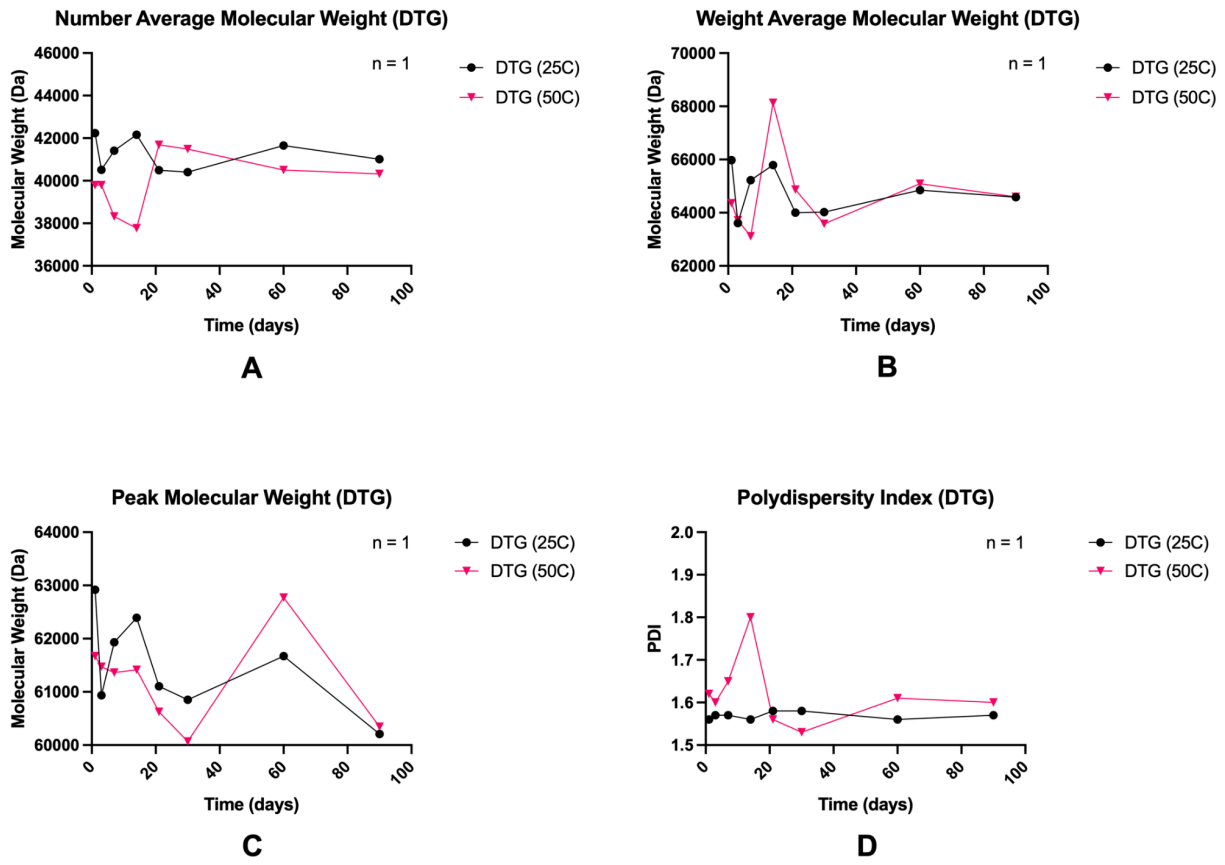

Figure 21: Molecular weight analysis graphs of DTG samples. (A) Number Average Molecular Weight (Mn). (B) Weight Average Molecular Weight (Mn). (C) Peak molecular Weight (Mp). (D) Polydispersity Index (PDI)

Looking at the results of the DTG samples (Figure 21), a different trend is observed. The Mn results (Figure 21A) show that the 50ºC DTG sample degrades slower than 25ºC samples for

most of the duration of the study. Furthermore, the Mn values are lower compared to those of the blank sample. While we might predict that drug-polymer interactions might slow down the degradation rate, it might appear that these interactions may actually speed up the degradation process. However, the Mw results show that the degradation rate is quite similar throughout the 3 month study, with no observable trend in the Mw, Mp, and PDI. By the end of the study, the values for these 3 characteristics are similar between the 25ºC and 50ºC samples. These results suggest that for samples containing DTG, there might not be any observable effect that the processing temperature has on the degradation rate at the end of 90 days.

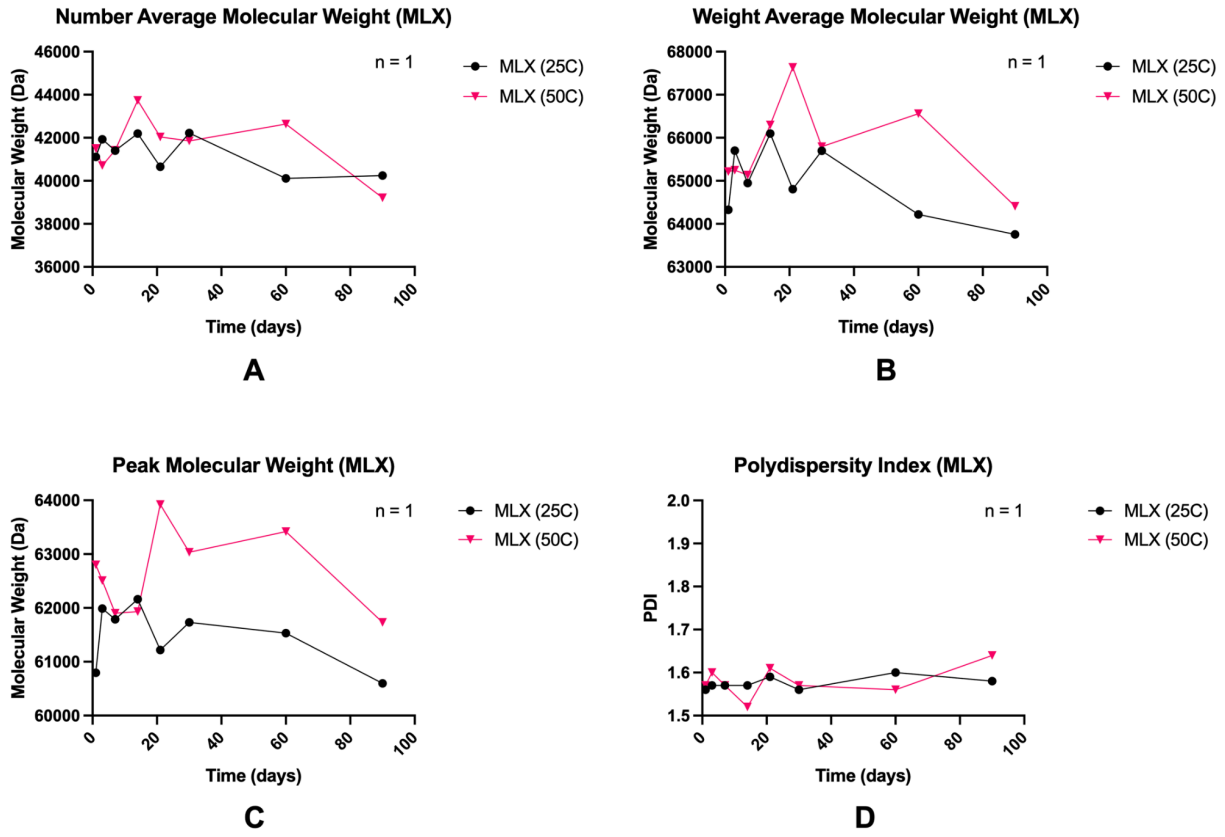

Figure 22: Molecular weight analysis graphs of MLX samples. (A) Number Average Molecular Weight (Mn). (B) Weight Average Molecular Weight (Mn). (C) Peak molecular Weight (Mp). (D) Polydispersity Index (PDI)

Interestingly, the MLX samples (Figure 22) seem to have a similar trend to the blank samples, where the 50ºC samples tends to have a higher molecular weight compared to the 25ºC samples, thereby suggesting a slower degradation rate. This can be seen across the Mw and Mp values, while the 50ºC samples have a slightly lower Mn than the 25ºC at the end of 90 days. However, this can be a result of longer polymer chains being broken down into shorter chains, skewing the Mn value lower. Nonetheless, the results suggest that PCL tablets containing MLX degrade slower when processed at 50ºC than when processed at 25ºC.

Within all sample compositions, we are not able to see a clear degradation trend over time, as Mw and Mn values are increasing and decreasing over time. Because samples were cut radially before being dissolved, a large proportion of the sample will have not been degraded. To achieve more accurate results of the degradation, it would be best to take a proportion of the sample that has more surface area, as opposed to the inner core portions that would degrade last.

Chapter 4: Conclusions

In conclusion, this project takes a deep dive into polymer morphology, particularly in the induction of mesophase on polymer blends and the study of degradation behaviors. By exploring the behavior and structures of Poly-L-Lactic Acid, Polycaprolactone, Polyethylene Oxide, and Poly-lactic-co-glycolic acid, the work we have done allows us to learn more about these polymers and how we can use them to our advantage in future projects. PLM images of birefringence without the presence of spherulites suggest a possible change in structure, while XRD confirmed our findings through Debye-Scherrer ring broadening. XRD peak deconvolution was able to quantify the phase content of these samples, suggesting that samples with higher PLA content exhibit increased mesophase content. On the flip side, PEO/PCL blends seem to maintain high levels of crystallinity with low mesophase formation. These findings highlight the role of polymer composition in morphological studies.

The PLGA degradation study allows us to study the effects that morphology has on degradation kinetics, which has not been previously studied. PLM images revealed the presence of crystalline structures in the typically amorphous PLGA samples during degradation, suggesting morphology/structural changes. GPC analysis further confirmed this phenomenon, as results find that films degrade slowest, followed by processed samples, and then unprocessed pellets. These findings suggest that processing is able to improve degradation rate compared to unprocessed samples, confirming our hypothesis that increasing order through mesophase induction would slow down degradation. This study further highlights the applications of polymer morphology, linking it directly with degradation. This work can be used to improve further medical implants used for human health.

The analysis of PCL tablets containing Dolutegravir and Meloxicam processed at different temperatures reveals that incorporation of drug can also affect the polymer morphology and degradation behavior. XRD and deconvolution results suggest minimal morphological changes over the course of the three-month study, due to the nature of PCL's slow degradation rate. GPC results show that samples did not exhibit a clear degradation trend, due to the section of the sample that was analyzed. Future experiments can look at analyzing areas primarily focusing on the surface of these tablets to gain a more accurate representation of the degradation. These results can further inform future research that can improve the drug delivery field.

Future experiments continuing these projects can use Differential Scanning Calorimetry to confirm the existence of mesophase through thermal analysis. Further analysis of the phase content results from each polymer can also be conducted to see which polymer might be playing a bigger role in the morphology of the respective tablet. Additionally, other polymer blends can be explored to investigate their ability to induce mesophase. Within the degradation studies, futere studies can be conducted to see if morphological or degradation behavior can be understood better over long-term periods. In the case of the slow-degrading PCL, more significant results may be obtained through a longer study.

In summary, this research is crucial in understanding polymer morphology and how it can be applied in various applications, such as biomedical innovations. Mesophase is a powerful, yet not well-known tool that can be used to augment the technologies that are used today. As such, the findings of this study are a huge step in understanding the field of polymers and serve as a strong foundation for future materials science and medical device research.

References

1. M. Aguilar, N., Perez-Aguilar, J.M., González-Coronel, V.J., Soriano Moro, J.G., and Sanchez-Gaytan, B.L. (2021). Polymers as Versatile Players in the Stabilization, Capping, and Design of Inorganic Nanostructures. ACS Omega *6*, 35196–35203. https://doi.org/10.1021/acsomega.1c05420.

2. Choi, K.Y. (2006). New Developments in Polymer Reaction Engineering. In Studies in Surface Science and Catalysis New Developments and Application in Chemical Reaction Engineering., H.-K. Rhee, I.-S. Nam, and J. M. Park, eds. (Elsevier), pp. 109–114. https://doi.org/10.1016/S0167-2991(06)81546-6.

3. Uttayarat, P., Perets, A., Li, M., Pimton, P., Stachelek, S.J., Alferiev, I., Composto, R.J., Levy, R.J., and Lelkes, P.I. (2010). Micropatterning of three-dimensional electrospun polyurethane vascular grafts. Acta Biomater. *6*, 4229–4237. https://doi.org/10.1016/j.actbio.2010.06.008.

4. Chung, S., Ingle, N.P., Montero, G.A., Kim, S.H., and King, M.W. (2010). Bioresorbable elastomeric vascular tissue engineering scaffolds via melt spinning and electrospinning. Acta Biomater. *6*, 1958–1967. https://doi.org/10.1016/j.actbio.2009.12.007.

5. Ertel, S.I., and Kohn, J. (1994). Evaluation of a series of tyrosine-derived polycarbonates as degradable biomaterials. J. Biomed. Mater. Res. *28*, 919–930. https://doi.org/10.1002/jbm.820280811.

6. Namazi, H. (2017). Polymers in our daily life. BioImpacts BI *7*, 73. https://doi.org/10.15171/bi.2017.09.

7. Fundamental Principles of Polymeric Materials https://platform.virdocs.com/read/548377/68/#/4/2.

8. Altshuler, G.B., and Tuchin, V.V. (2009). Chapter 3 - Physics Behind Light-Based Systems: Skin and Hair Follicle Interactions with Light. In Cosmetics Applications of Laser & Light-Based Systems Personal Care & Cosmetic Technology., G. S. Ahluwalia, ed. (William Andrew Publishing), pp. 49–123. https://doi.org/10.1016/B978-0-8155-1572-2.50008-7.

9. Li, S. (2008). *In vitro* physicochemical test methods to evaluate bioresorbability. In Degradation Rate of Bioresorbable Materials Woodhead Publishing Series in Biomaterials., F. Buchanan, ed. (Woodhead Publishing), pp. 117–144. https://doi.org/10.1533/9781845695033.3.117.

10. Baptista, C., Azagury, A., Shin, H., Baker, C.M., Ly, E., Lee, R., and Mathiowitz, E. (2020). The effect of temperature and pressure on polycaprolactone morphology. Polymer *191*, 122227. https://doi.org/10.1016/j.polymer.2020.122227.

11. Baker, C.M., Azagury, A., and Mathiowitz, E. (2016). Effect of pressure on poly-l-Lactic

Acid morphology. Polymer *99*, 250–262. https://doi.org/10.1016/j.polymer.2016.07.028.

12. Baptista, C., Azagury, A., Baker, C.M., and Mathiowitz, E. (2021). The characterization and quantification of the induced mesophases of poly-l-lactic acid. Polymer *226*, 123822. https://doi.org/10.1016/j.polymer.2021.123822.

13. Nair, N.R., Sekhar, V.C., Nampoothiri, K.M., and Pandey, A. (2017). 32 - Biodegradation of Biopolymers. In Current Developments in Biotechnology and Bioengineering, A. Pandey, S. Negi, and C. R. Soccol, eds. (Elsevier), pp. 739–755. https://doi.org/10.1016/B978-0-444-63662-1.00032-4.

14. Endres, H.-J., and Siebert-Raths, A. (2012). 10.19 - Performance Profile of Biopolymers Compared to Conventional Plastics. In Polymer Science: A Comprehensive Reference, K. Matyjaszewski and M. Möller, eds. (Elsevier), pp. 317–353. https://doi.org/10.1016/B978-0-444-53349-4.00270-3.

15. Zaroog, O.S., Borhana, A.A., and Perumal, S.S.A. (2019). Biomaterials for Bone Replacements: Past and Present. In Reference Module in Materials Science and Materials Engineering (Elsevier). https://doi.org/10.1016/B978-0-12-803581-8.11442-0.

16. Deshmukh, K., Basheer Ahamed, M., Deshmukh, R.R., Khadheer Pasha, S.K., Bhagat, P.R., and Chidambaram, K. (2017). 3 - Biopolymer Composites With High Dielectric Performance: Interface Engineering. In Biopolymer Composites in Electronics, K. K. Sadasivuni, D. Ponnamma, J. Kim, J.-J. Cabibihan, and M. A. AlMaadeed, eds. (Elsevier), pp. 27–128. https://doi.org/10.1016/B978-0-12-809261-3.00003-6.

17. Manivasagam, G., Reddy, A., Sen, D., Nayak, S., Mathew, M.T., and Rajamanikam, A. (2019). Dentistry: Restorative and Regenerative Approaches. In Encyclopedia of Biomedical Engineering, R. Narayan, ed. (Elsevier), pp. 332–347. https://doi.org/10.1016/B978-0-12-801238-3.11017-7.

18. Christen, M.-O., and Vercesi, F. (2020). Polycaprolactone: How a Well-Known and Futuristic Polymer Has Become an Innovative Collagen-Stimulator in Esthetics. Clin. Cosmet. Investig. Dermatol. *13*, 31. https://doi.org/10.2147/CCID.S229054.

19. Dwivedi, R., Kumar, S., Pandey, R., Mahajan, A., Nandana, D., Katti, D.S., and Mehrotra, D. (2020). Polycaprolactone as biomaterial for bone scaffolds: Review of literature. J. Oral Biol. Craniofacial Res. *10*, 381–388. https://doi.org/10.1016/j.jobcr.2019.10.003.

20. Sharifi, S., Mirzadeh, H., Imani, M., Rong, Z., Jamshidi, A., Shokrgozar, M., Atai, M., and Roohpour, N. (2009). Injectable in situ forming drug delivery system based on poly(ε-caprolactone fumarate) for tamoxifen citrate delivery: Gelation characteristics, in vitro drug release and anti-cancer evaluation. Acta Biomater. *5*, 1966–1978. https://doi.org/10.1016/j.actbio.2009.02.004.

21. Li, R., Li, X., Xie, L., Ding, D., Hu, Y., Qian, X., Yu, L., Ding, Y., Jiang, X., and Liu, B.

(2009). Preparation and evaluation of PEG–PCL nanoparticles for local tetradrine delivery. Int. J. Pharm. *379*, 158–166. https://doi.org/10.1016/j.ijpharm.2009.06.007.

22. Ayvazoğlu, B.Ş., Ceylan, M., Turan, A.A.I., and Yılmaz, E.B. (2023). Biodegradable Polycaprolactone Fibers with Silica Aerogel and Nanosilver Particles Produce a Coagulation Effect. Polymers *15*, 2022. https://doi.org/10.3390/polym15092022.

23. Abdullah, T., Gauthaman, K., Mostafavi, A., Alshahrie, A., Salah, N., Morganti, P., Chianese, A., Tamayol, A., and Memic, A. (2020). Sustainable drug release from polycaprolactone coated chitin-lignin gel fibrous scaffolds. Sci. Rep. *10*, 20428. https://doi.org/10.1038/s41598-020-76971-w.

24. Tang, X., Thankappan, S.K., Lee, P., Fard, S.E., Harmon, M.D., Tran, K., and Yu, X. (2014). Chapter 21 - Polymeric Biomaterials in Tissue Engineering and Regenerative Medicine. In Natural and Synthetic Biomedical Polymers, S. G. Kumbar, C. T. Laurencin, and M. Deng, eds. (Elsevier), pp. 351–371. https://doi.org/10.1016/B978-0-12-396983-5.00022-3.

25. Mehdipour-Ataei, S., and Mohammadi, M. (2023). 9 - Modification of unsaturated polyester resin by poly (ethylene glycol). In Applications of Unsaturated Polyester Resins, S. Thomas and C. J. Chirayil, eds. (Elsevier), pp. 141–153. https://doi.org/10.1016/B978-0-323-99466-8.00010-1.

26. Car, A. (2016). Polyethylene Oxide. In Encyclopedia of Membranes, E. Drioli and L. Giorno, eds. (Springer), pp. 1–2. https://doi.org/10.1007/978-3-642-40872-4_480-2.

27. Polaskova, M., Peer, P., Cermak, R., and Ponizil, P. (2019). Effect of Thermal Treatment on Crystallinity of Poly(ethylene oxide) Electrospun Fibers. Polymers *11*, 1384. https://doi.org/10.3390/polym11091384.

28. Poly(ethylene oxide), MW 100000 (PEO 100K) https://www.polysciences.com/default/polyethylene-oxide-mw100000.

29. Stella, V.J. (2013). Chemical Drug Stability in Lipids, Modified Lipids, and Polyethylene Oxide-Containing Formulations. Pharm. Res. *30*, 3018–3028. https://doi.org/10.1007/s11095-013-1051-2.

30. Körner, A., Larsson, A., Piculell, L., and Wittgren, B. (2005). Molecular information on the dissolution of polydisperse polymers: Mixtures of long and short poly(ethylene oxide). J. Phys. Chem. B *109*, 11530–11537. https://doi.org/10.1021/jp044332s.

31. Miro, A., Rondinone, A., Nappi, A., Ungaro, F., Quaglia, F., and La Rotonda, M.I. (2009). Modulation of release rate and barrier transport of Diclofenac incorporated in hydrophilic matrices: role of cyclodextrins and implications in oral drug delivery. Eur. J. Pharm. Biopharm. Off. J. Arbeitsgemeinschaft Pharm. Verfahrenstechnik EV *72*, 76–82. https://doi.org/10.1016/j.ejpb.2008.12.006.

32. Patra, A.K., and Pattanayak, A.K. (2015). 16 - Novel varieties of denim fabrics. In Denim

Woodhead Publishing Series in Textiles., R. Paul, ed. (Woodhead Publishing), pp. 483–506. https://doi.org/10.1016/B978-0-85709-843-6.00016-0.

33. Marek, A.A., and Verney, V. (2016). Photochemical reactivity of PLA at the vicinity of glass transition temperature. The photo-rheology method. Eur. Polym. J. *81*, 239–246. https://doi.org/10.1016/j.eurpolymj.2016.06.016.

34. Polygenis, T. A Comprehensive Guide to PLA Melting Point and How it Influences 3D Printing. https://www.wevolver.com/article/a-comprehensive-guide-to-pla-melting-point-and-how-it-influences-3d-printing.

35. Durand, B., and Marchand, C. (2016). 13 - Smart features in fibrous implantable medical devices. In Smart Textiles and their Applications Woodhead Publishing Series in Textiles., V. Koncar, ed. (Woodhead Publishing), pp. 257–307. https://doi.org/10.1016/B978-0-08-100574-3.00013-8.

36. L, D., M, D., H, H., H, P., Le, C., and A, I. (2001). Resorbable polymer fibers for ligament augmentation. J. Biomed. Mater. Res. *58*. https://doi.org/10.1002/jbm.1067.

37. K, U., K, H., Y, I., J, Y., T, H., Y, T., H, O., T, F., and M, S. (2005). Cartilage regeneration using mesenchymal stem cells and a three-dimensional poly-lactic-glycolic acid (PLGA) scaffold. Biomaterials *26*. https://doi.org/10.1016/j.biomaterials.2004.10.037.

38. Sj, P., Mj, M., Aw, Y., Mj, Y., and Ag, M. (1998). Polymer concepts in tissue engineering. J. Biomed. Mater. Res. *43*. https://doi.org/10.1002/(sici)1097-4636(199824)43:4<422::aid-jbm9>3.0.co;2-1.

39. S, C., T, Y., M, L., Lh, H., and R, L. (1991). Controlled delivery systems for proteins based on poly(lactic/glycolic acid) microspheres. Pharm. Res. *8*. https://doi.org/10.1023/a:1015841715384.

40. Houchin, M.L., and Topp, E.M. (2009). Physical properties of PLGA films during polymer degradation. J. Appl. Polym. Sci. *114*, 2848–2854. https://doi.org/10.1002/app.30813.

41. Gentile, P., Chiono, V., Carmagnola, I., and Hatton, P.V. (2014). An Overview of Poly(lactic-co-glycolic) Acid (PLGA)-Based Biomaterials for Bone Tissue Engineering. Int. J. Mol. Sci. *15*, 3640–3659. https://doi.org/10.3390/ijms15033640.

42. Potential Roles of the Glass Transition Temperature of PLGA Microparticles in Drug Release Kinetics | Molecular Pharmaceutics https://pubs-acs-org.revproxy.brown.edu/doi/10.1021/acs.molpharmaceut.0c01089.

43. Lanao, R.P.F., Jonker, A.M., Wolke, J.G., Jansen, J.A., Hest, J.C. van, and Leeuwenburgh, S.C. (2013). Physicochemical Properties and Applications of Poly(lactic-co-glycolic acid) for Use in Bone Regeneration. Tissue Eng. Part B Rev. *19*, 380. https://doi.org/10.1089/ten.teb.2012.0443.

44. Kumar, K.K., Ravi, M., Pavani, Y., Bhavani, S., Sharma, A.K., and Narasimha Rao, V.V.R. (2014). Investigations on PEO/PVP/NaBr complexed polymer blend electrolytes for electrochemical cell applications. J. Membr. Sci. *454*, 200–211. https://doi.org/10.1016/j.memsci.2013.12.022.

45. Dias, J.R., Sousa, A., Augusto, A., Bártolo, P.J., and Granja, P.L. (2022). Electrospun Polycaprolactone (PCL) Degradation: An In Vitro and In Vivo Study. Polymers *14*, 3397. https://doi.org/10.3390/polym14163397.

Appendix A

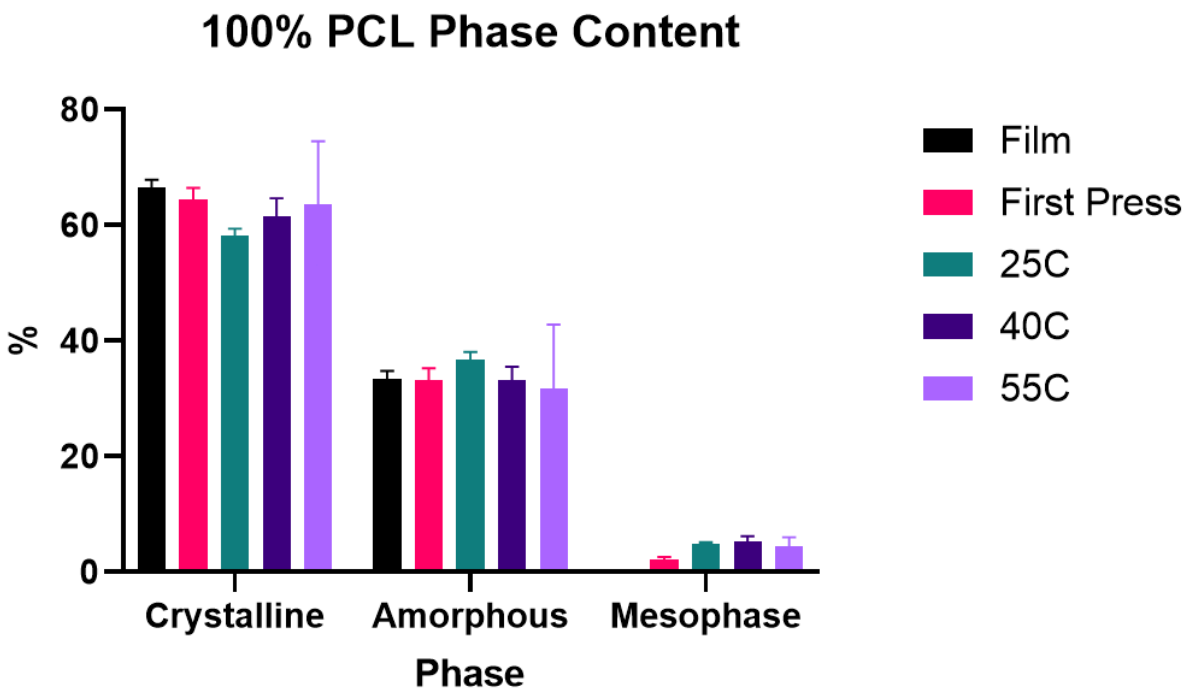

Supplementary Figure 1: 100% PCL Phase Content Graph

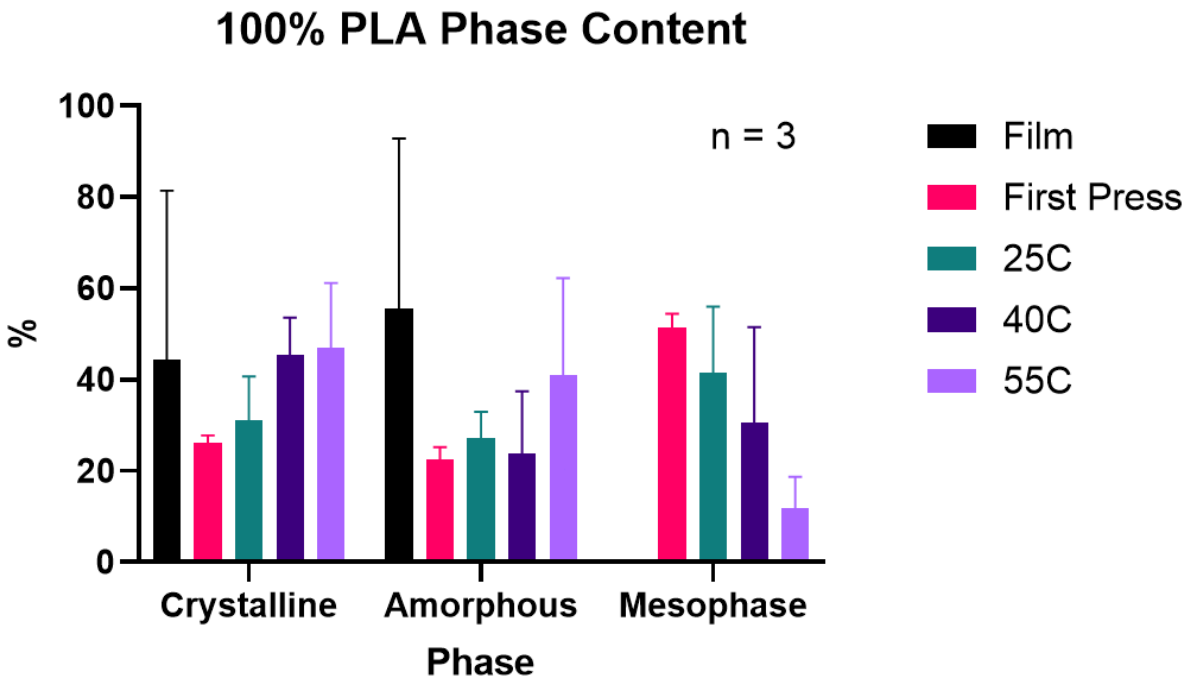

Supplementary Figure 2: 100% PLA Phase Content Graph

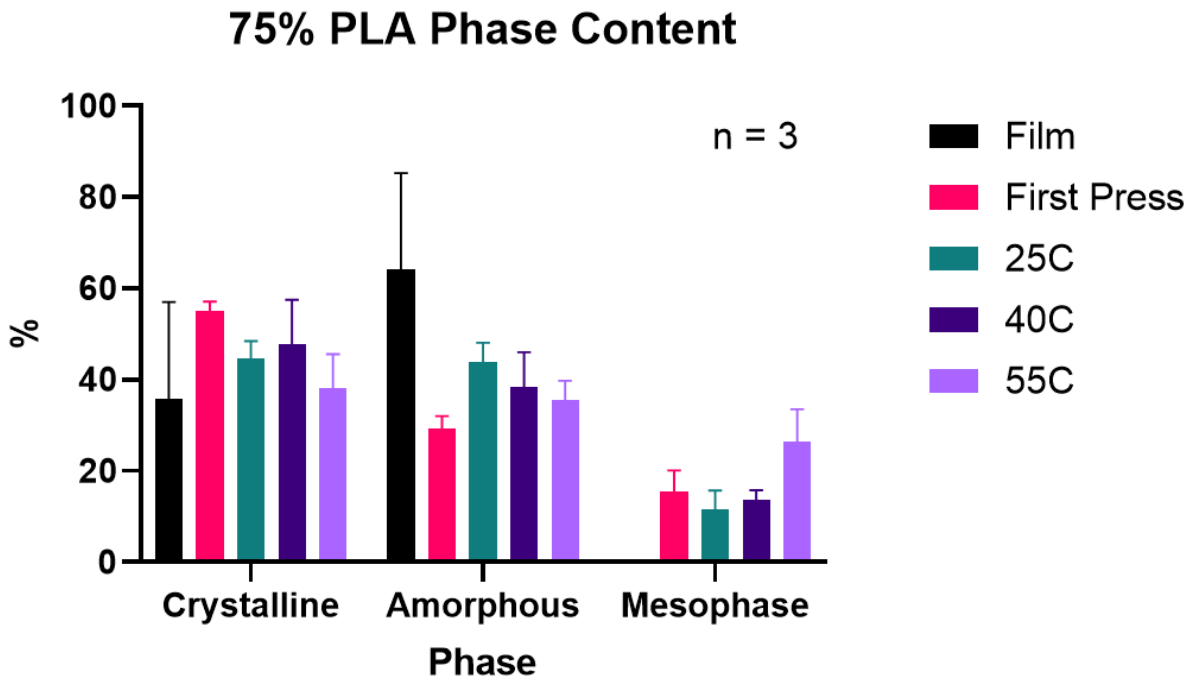

Supplementary Figure 3: 75% PLA Phase Content Graph

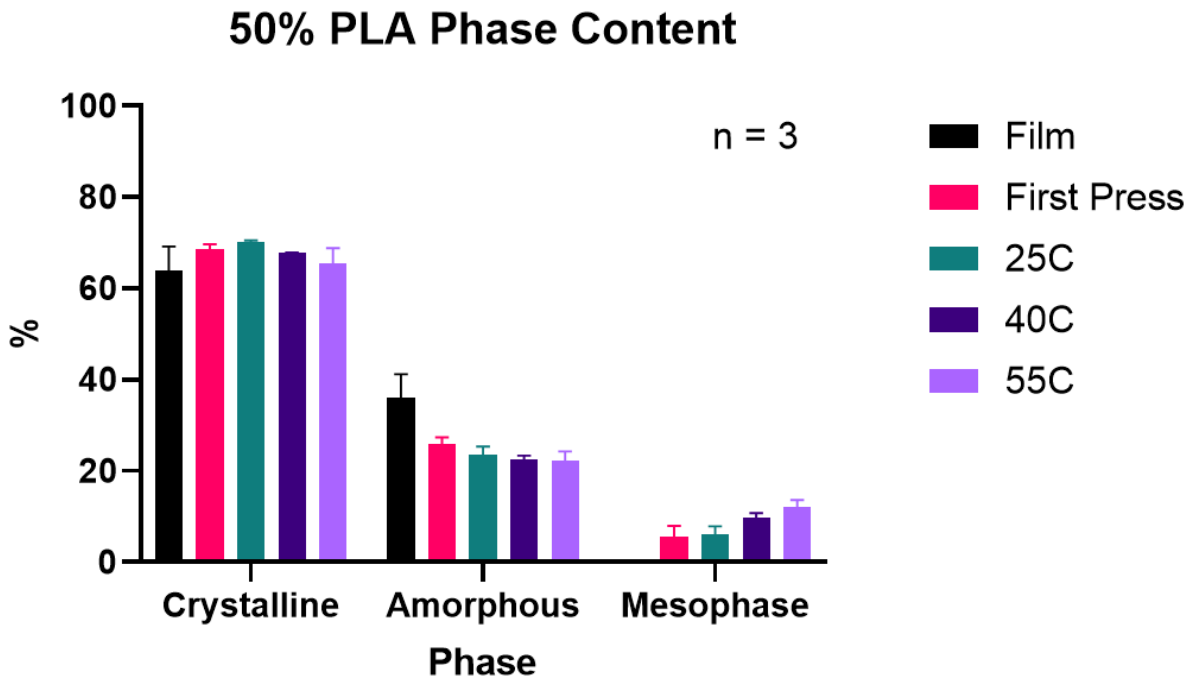

Supplementary Figure 4: 50% PLA Phase Content Graph

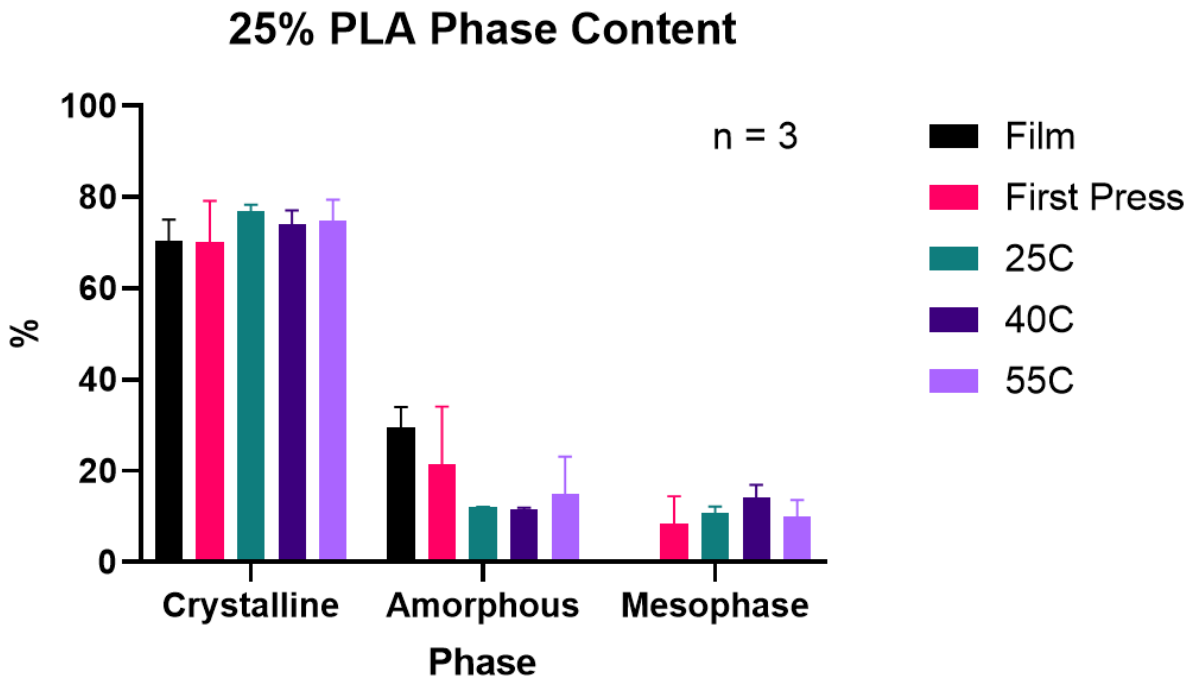

Supplementary Figure 5: 25% PLA Phase Content Graph

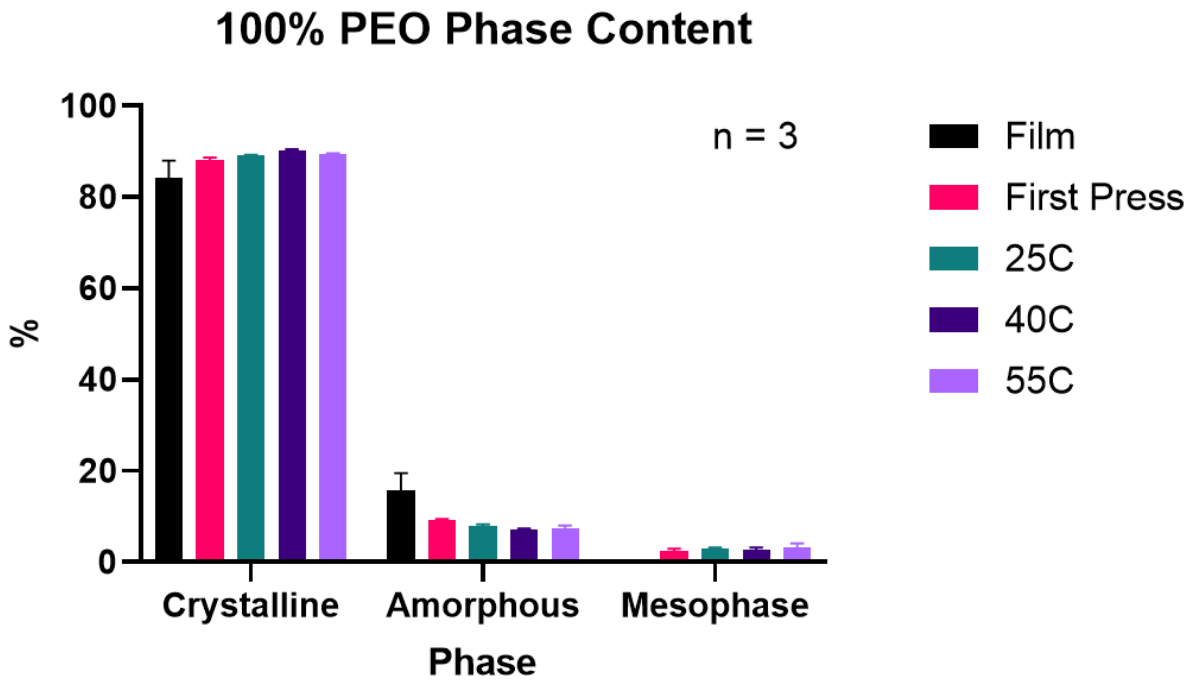

Supplementary Figure 6: 100% PEO Phase Content Graph

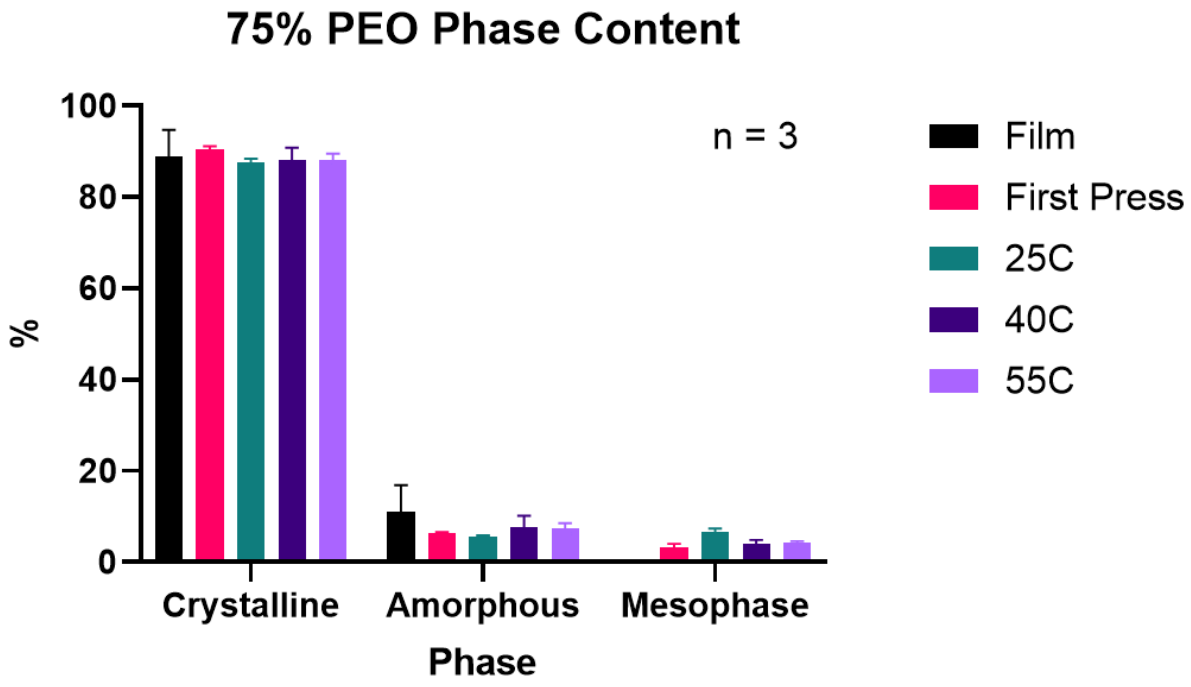

Supplementary Figure 7: 75% PEO Phase Content Graph

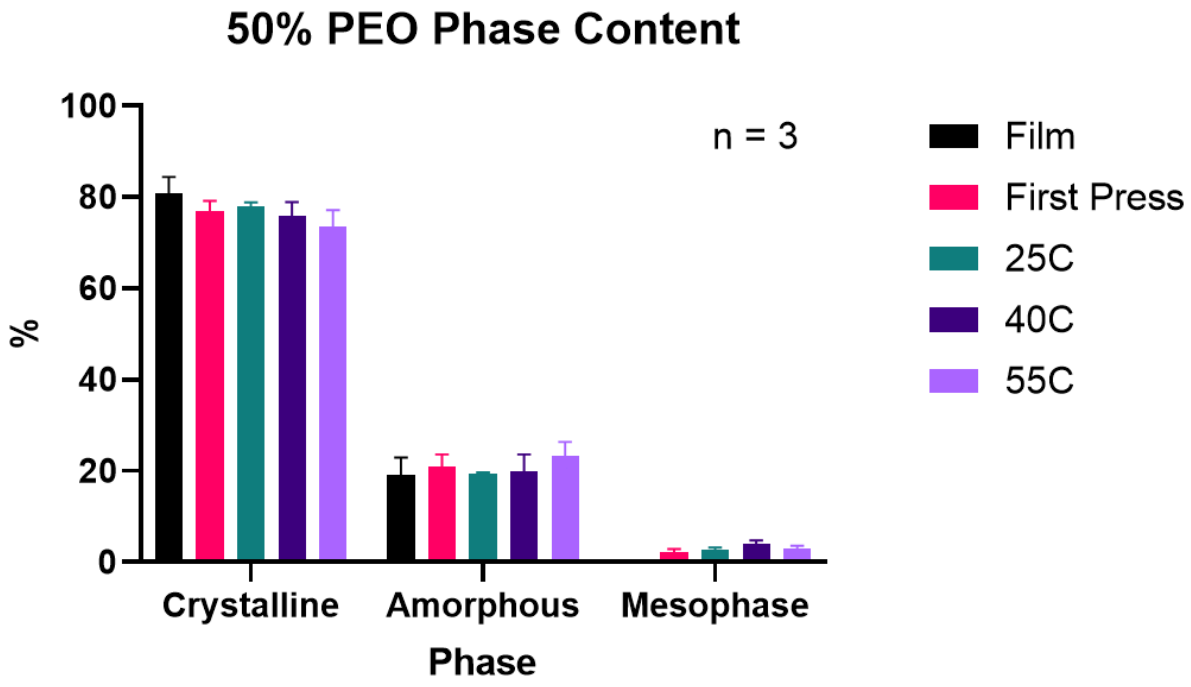

Supplementary Figure 8: 50% PEO Phase Content Graph

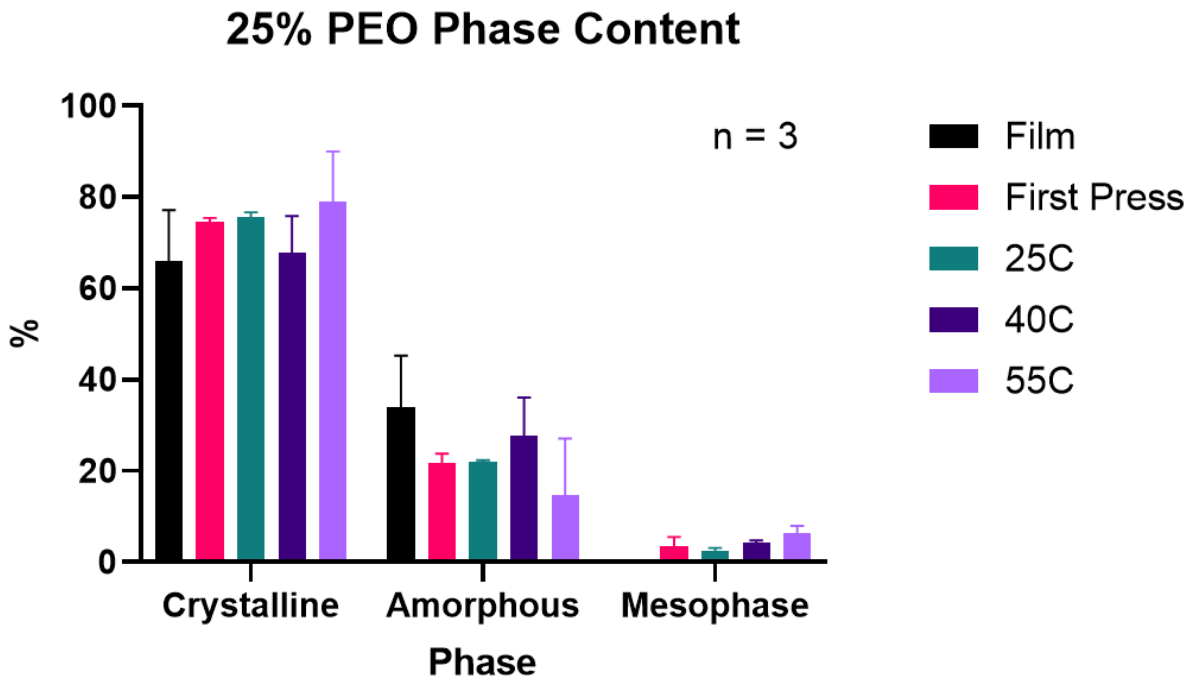

Supplementary Figure 9: 25% PEO Phase Content Graph

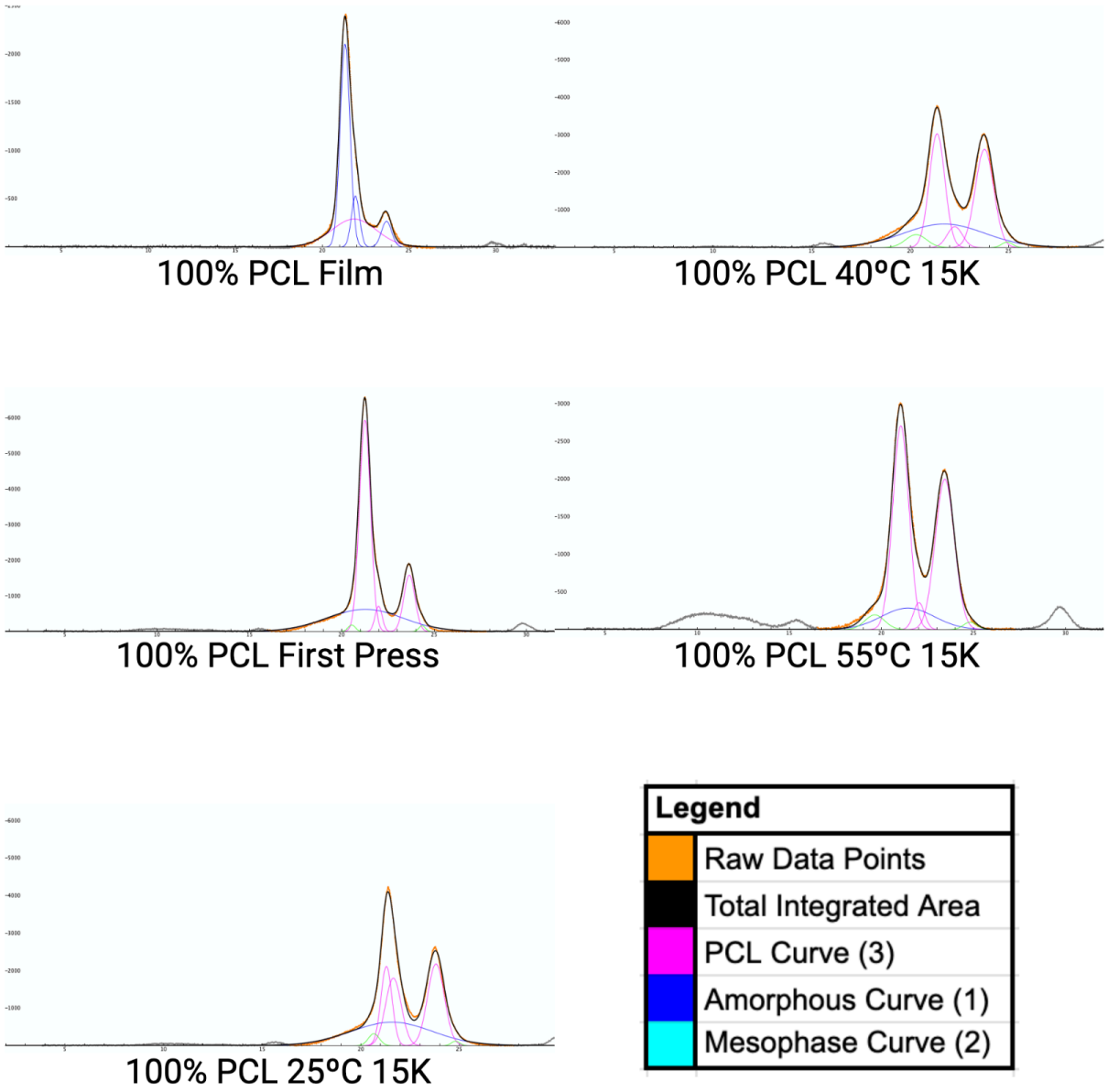

Supplementary Figure 10: Deconvolution Graphs of 100% PCL samples at different processing conditions.

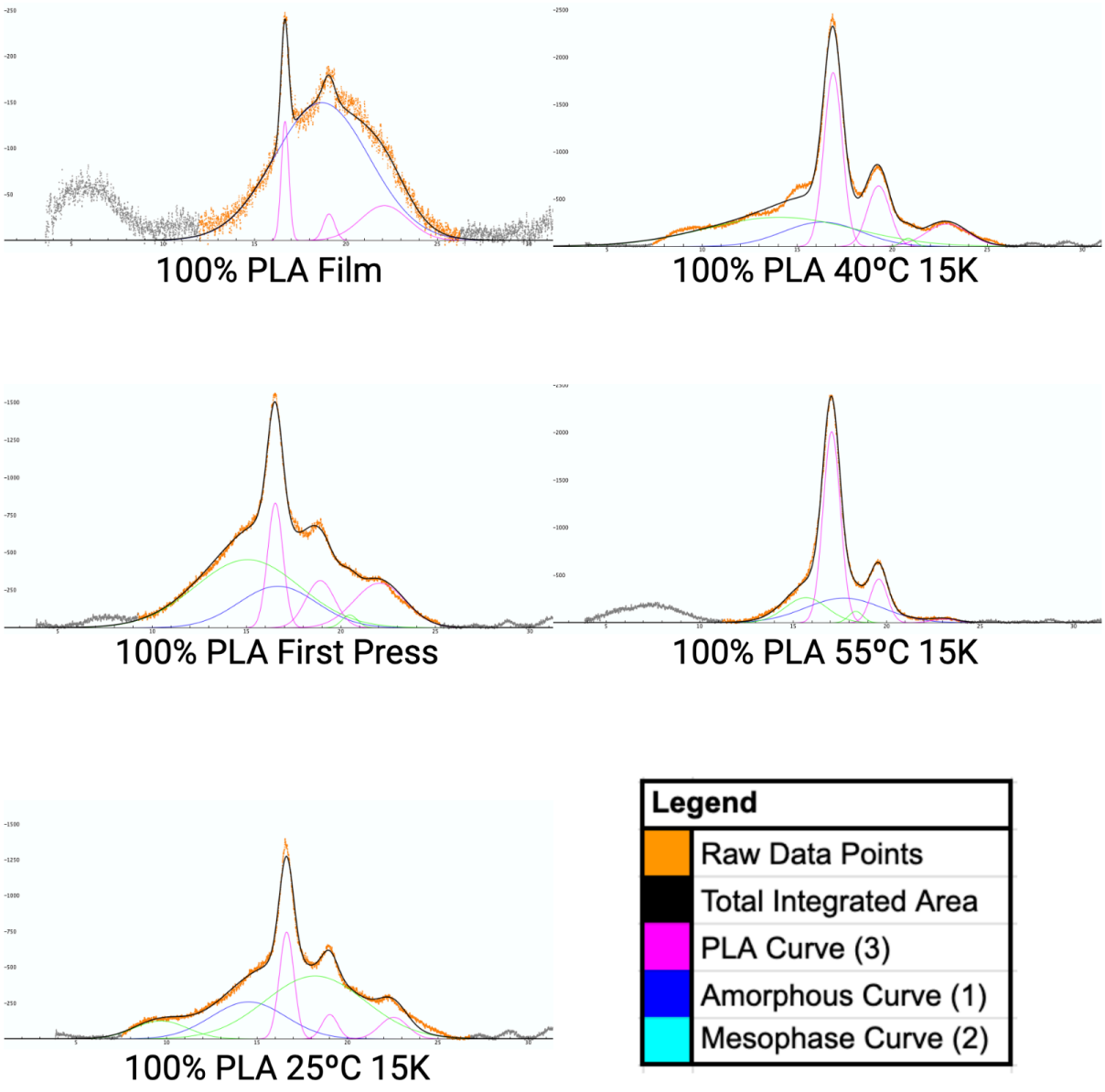

Supplementary Figure 11: Deconvolution Graphs of 100% PLA samples at different processing conditions.

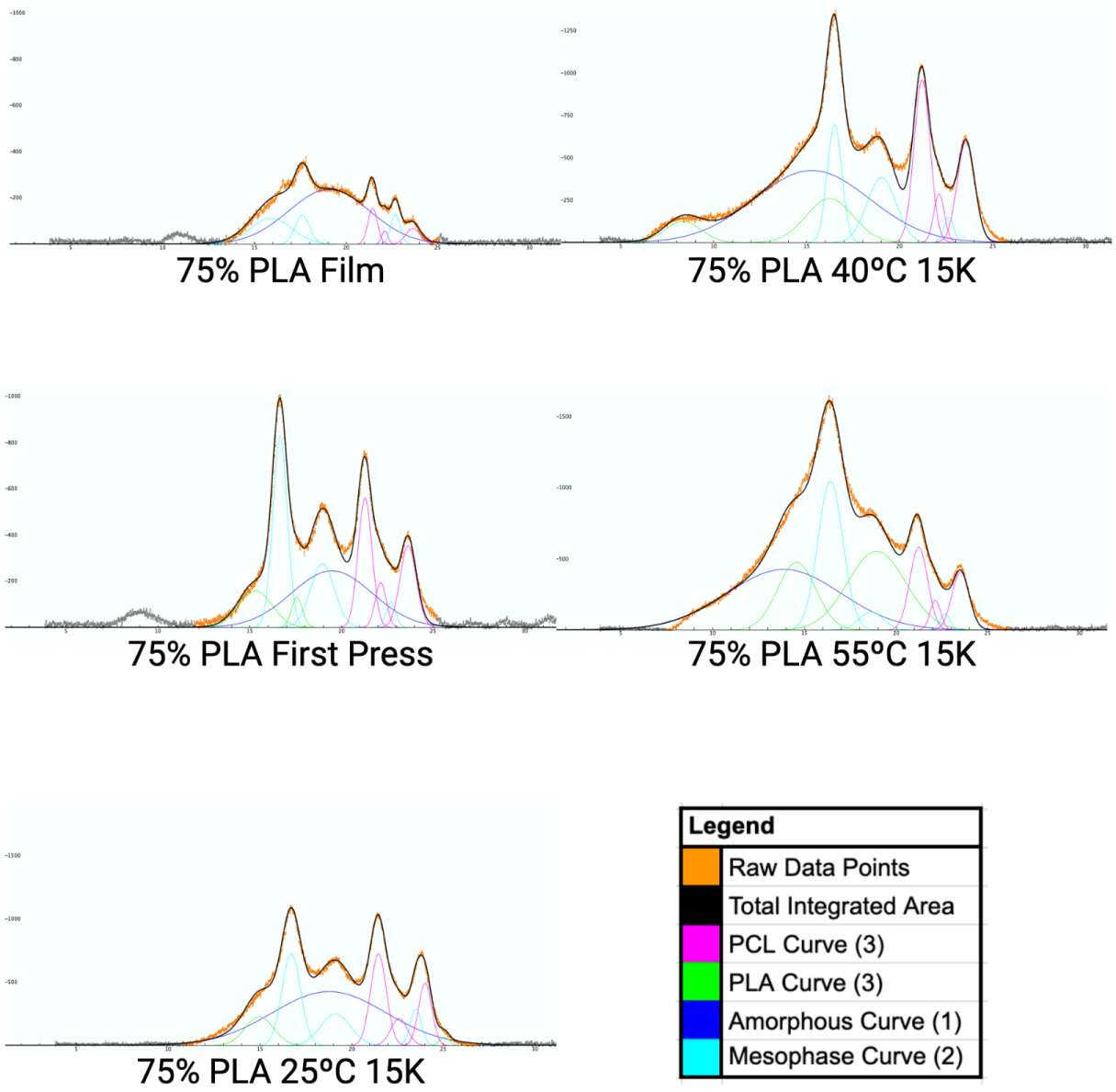

Supplementary Figure 12: Deconvolution Graphs of 75% PLA, 25% PCL samples at different processing conditions.

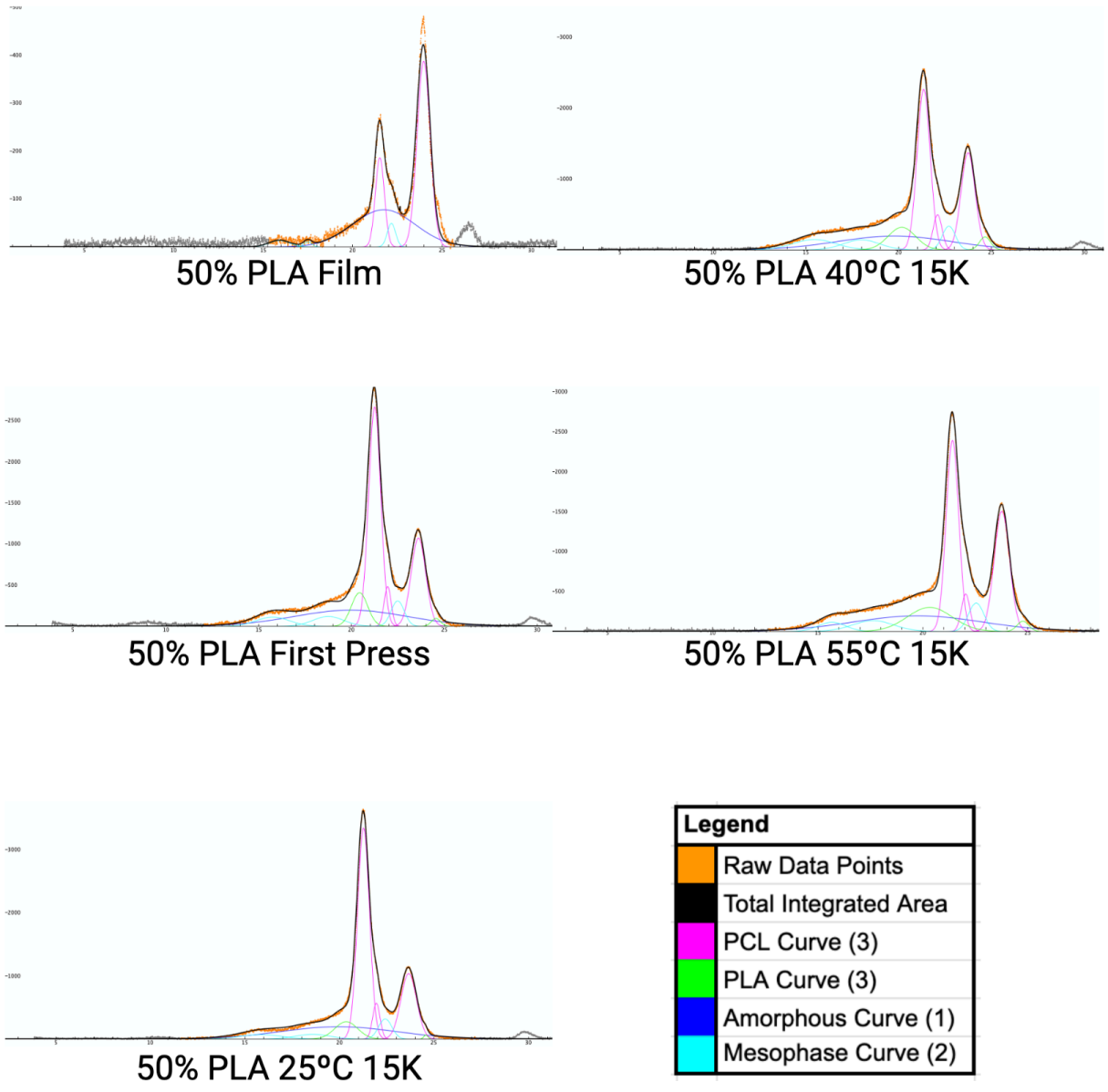

Supplementary Figure 13: Deconvolution Graphs of 50% PLA, 50% PCL samples at different processing conditions.

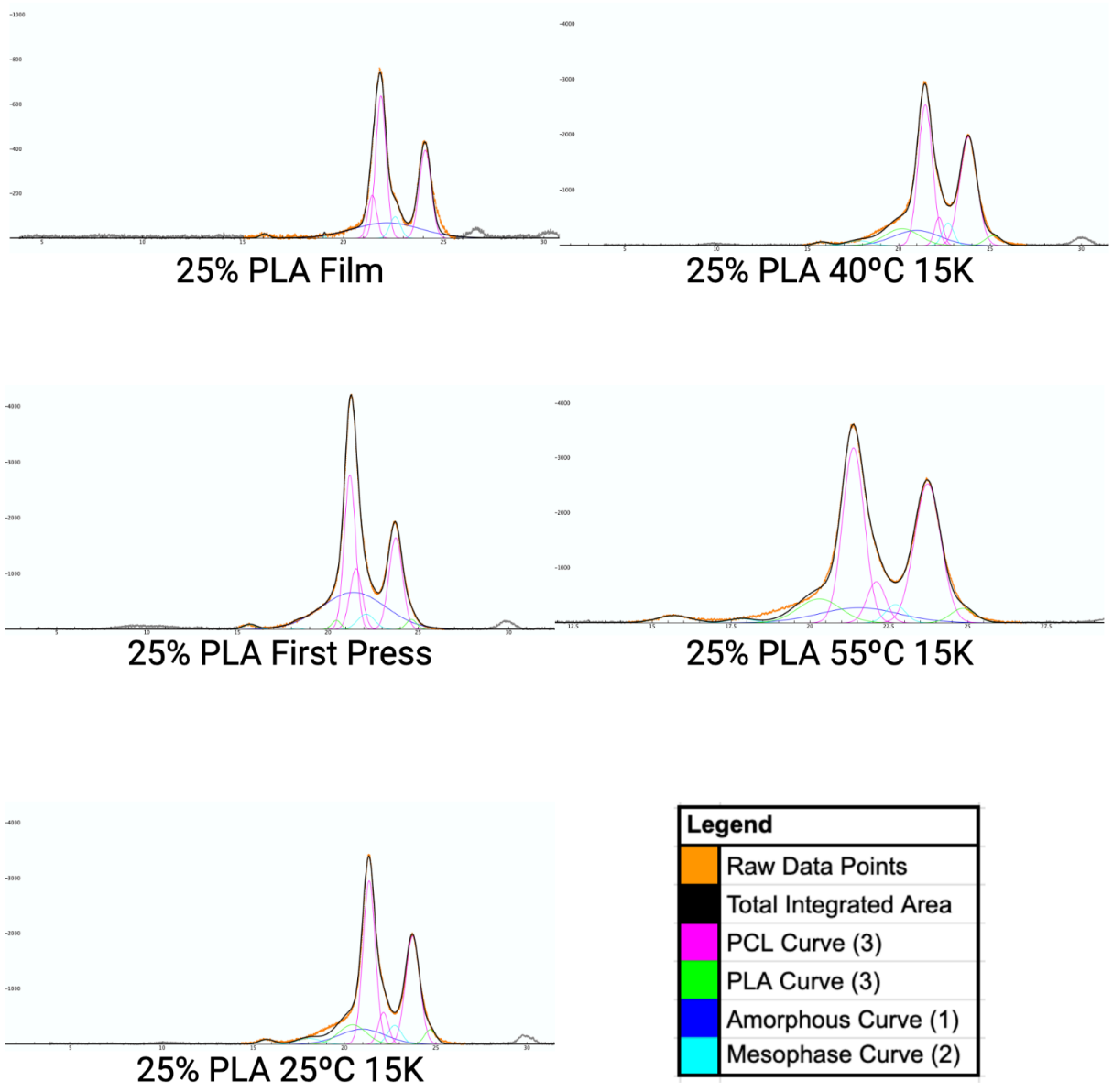

Supplementary Figure 14: Deconvolution Graphs of 25% PLA, 75% PCL samples at different processing conditions.

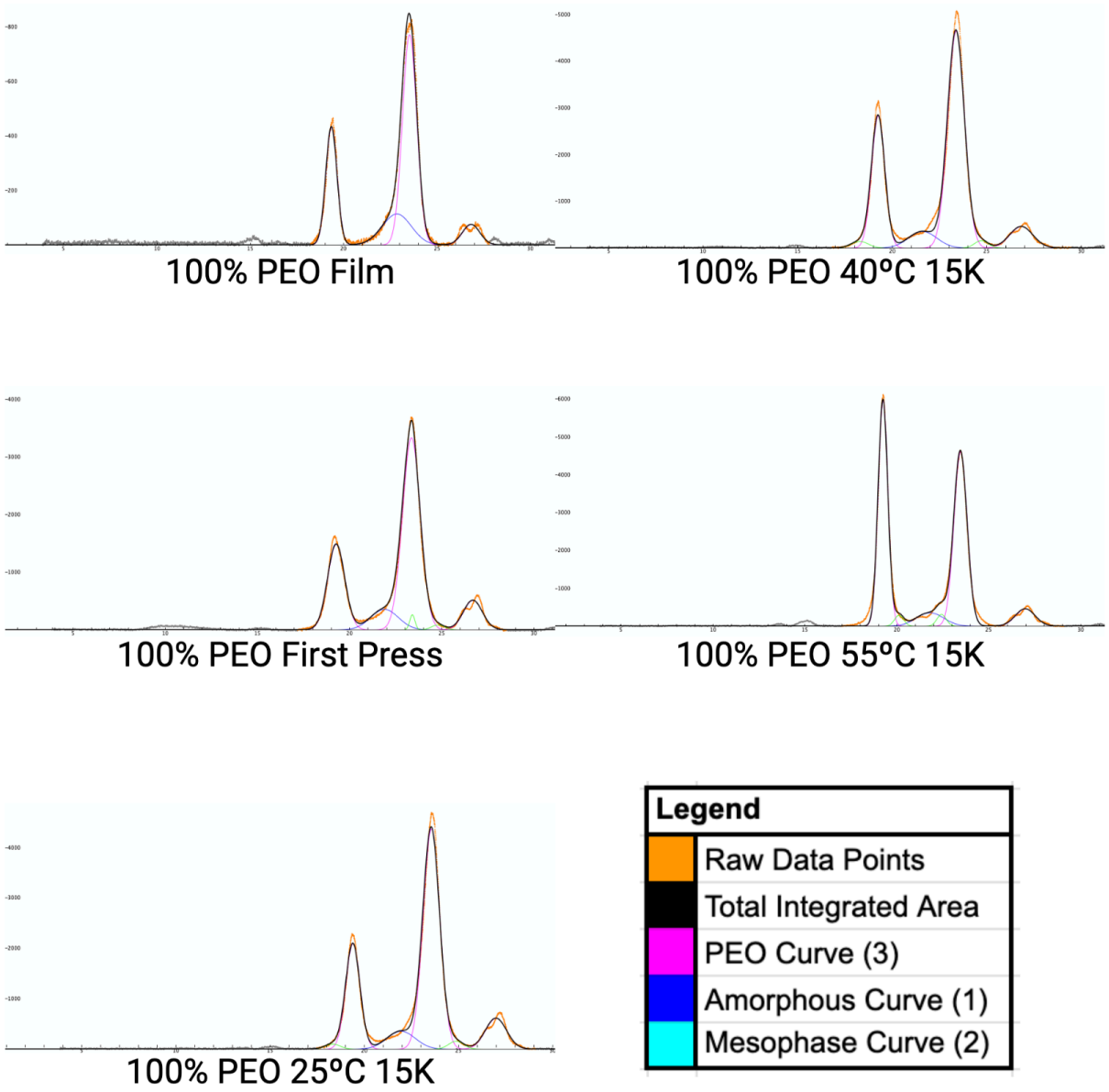

Supplementary Figure 15: Deconvolution Graphs of 100% PEO samples at different processing conditions.

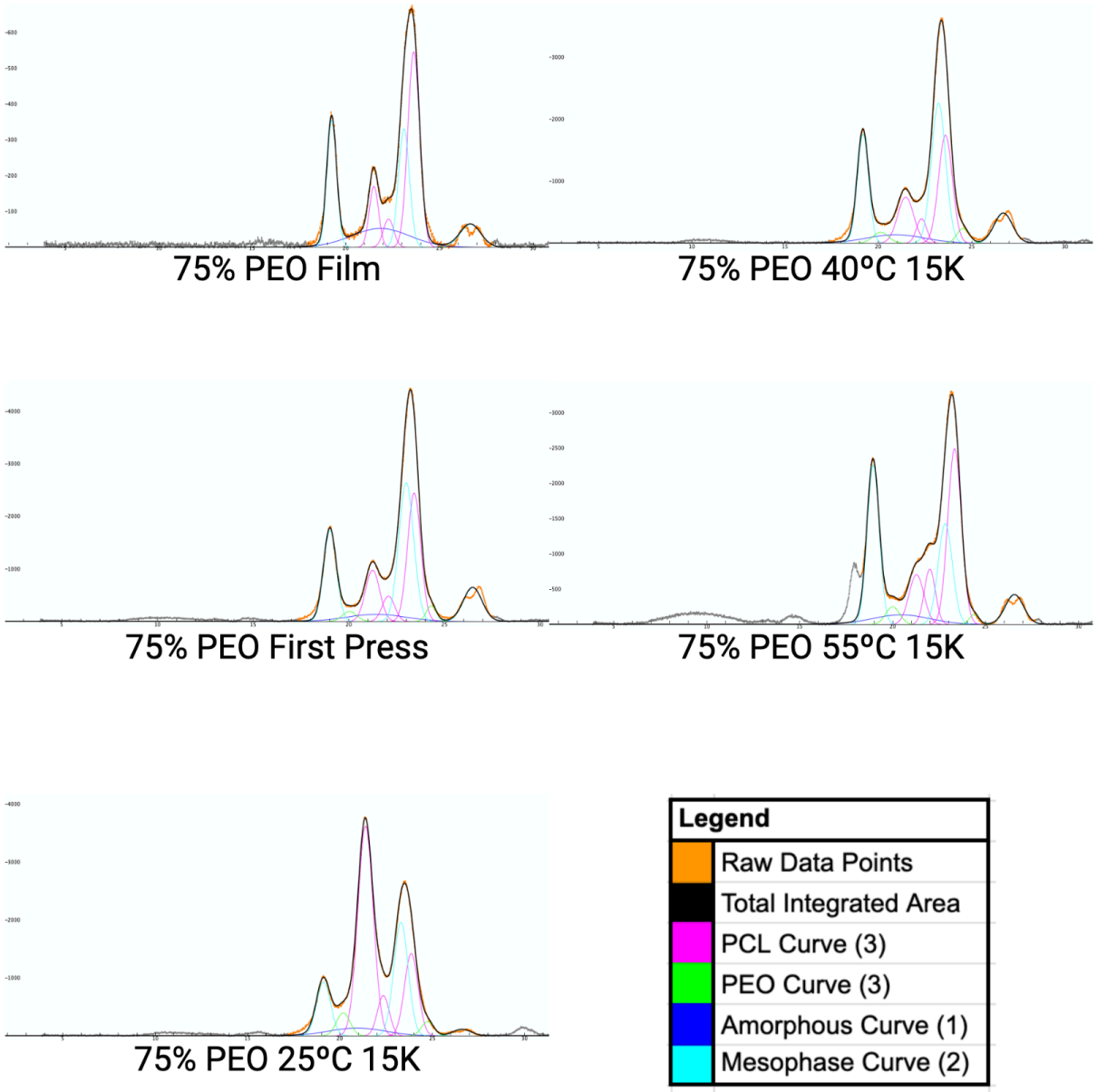

Supplementary Figure 16: Deconvolution Graphs of 75% PEO, 25% PCL samples at different processing conditions.

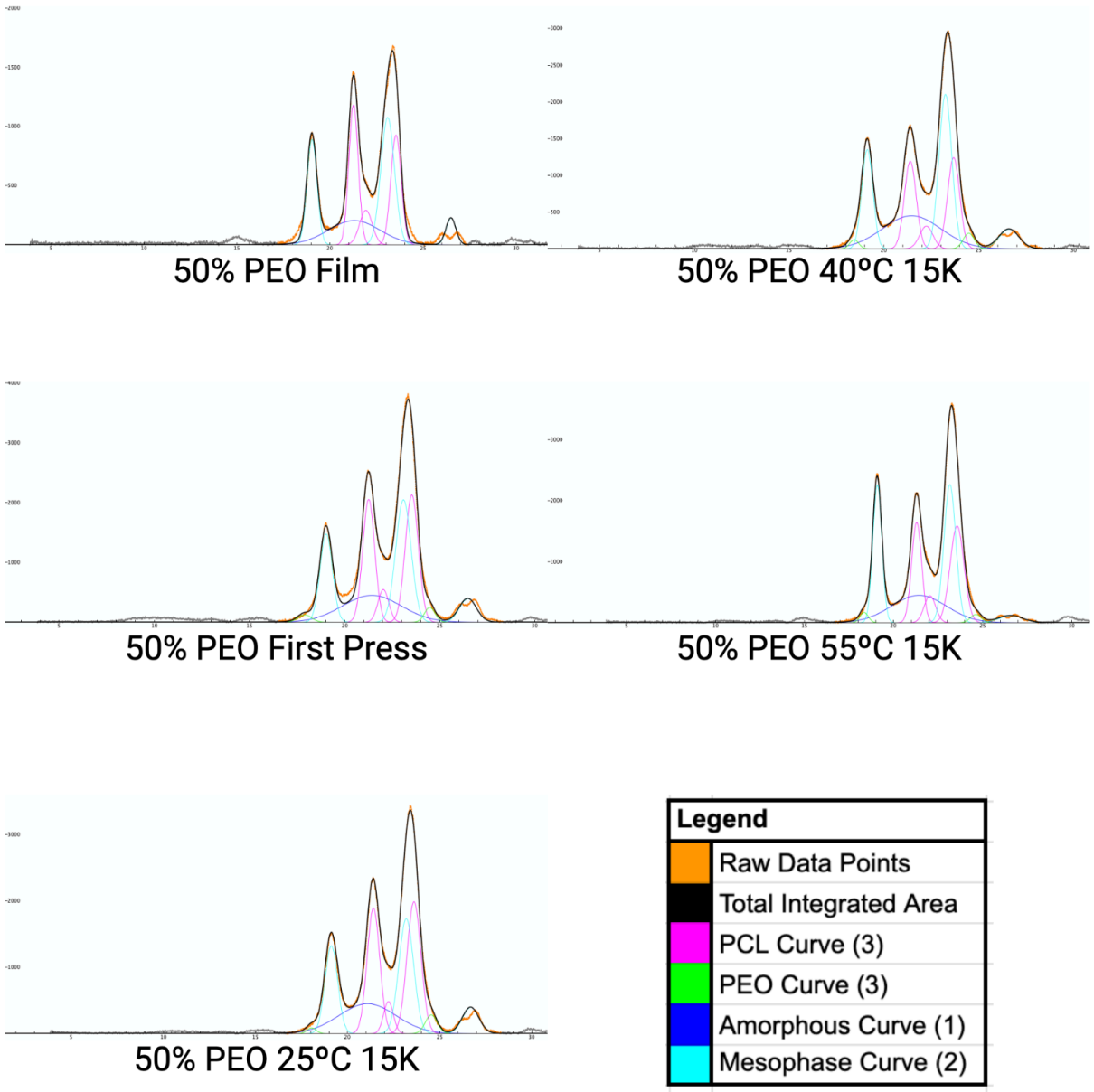

Supplementary Figure 17: Deconvolution Graphs of 50% PEO, 50% PCL samples at different processing conditions.

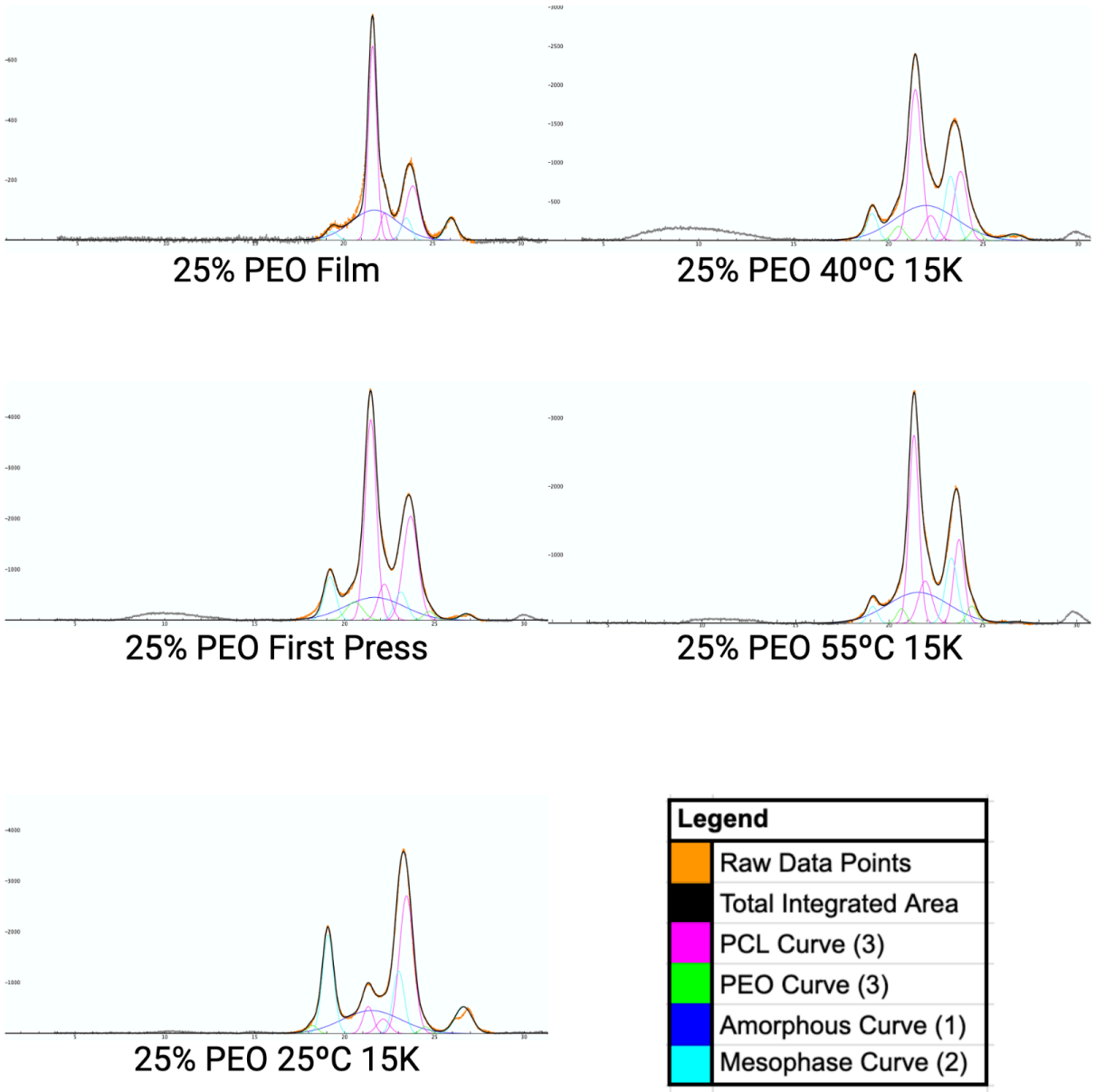

Supplementary Figure 18: Deconvolution Graphs of 25% PEO, 75% PCL samples at different processing conditions.

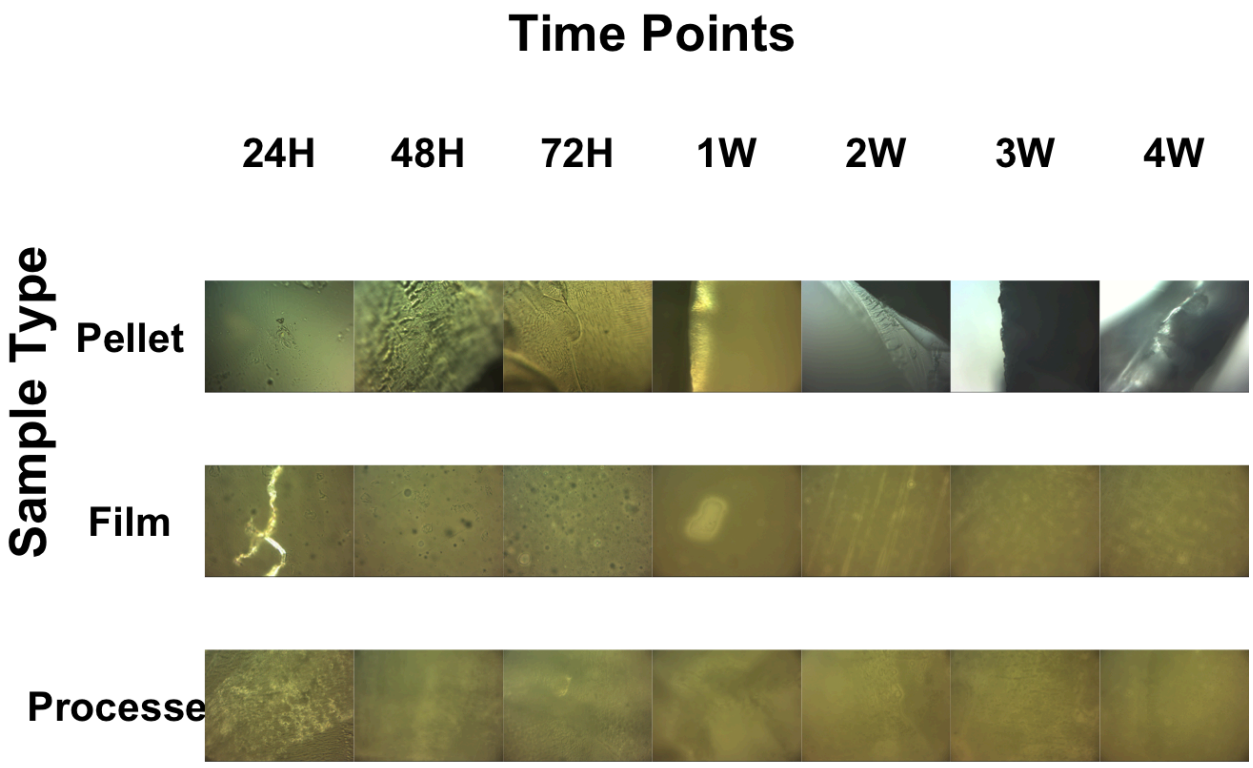

Supplementary Figure 19: PLM Images of degraded PLGA samples at 40x magnification

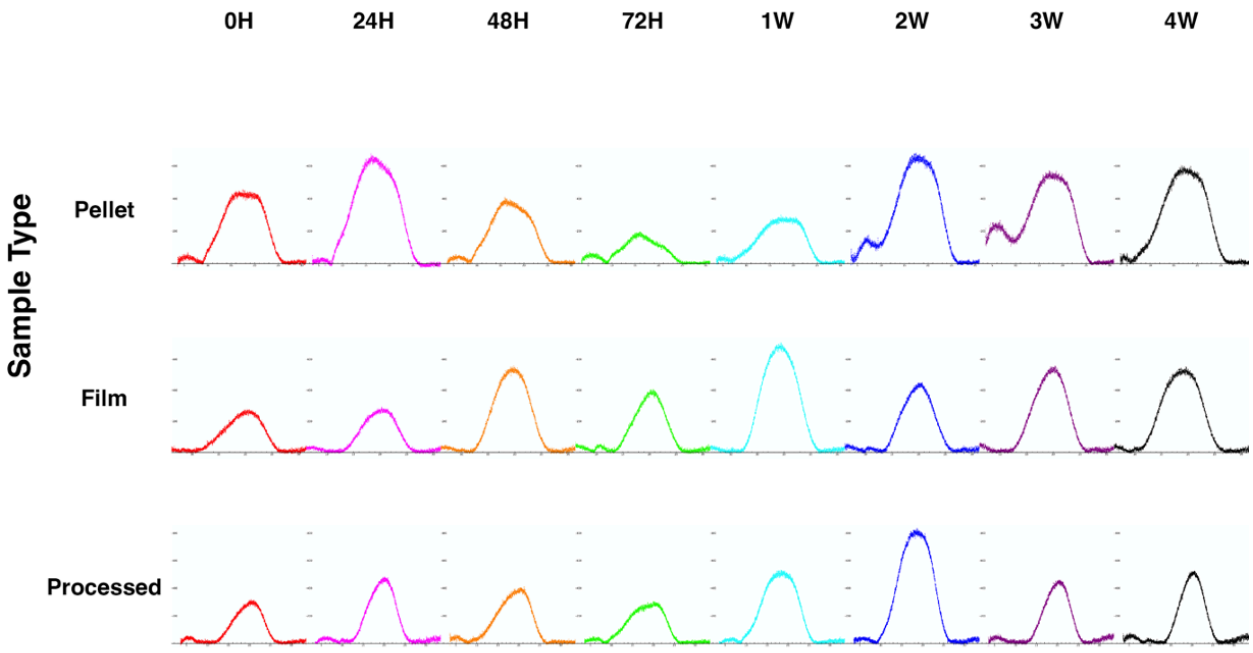

Supplementary Figure 20: Table comparing XRD scans of different PLGA processing conditions.

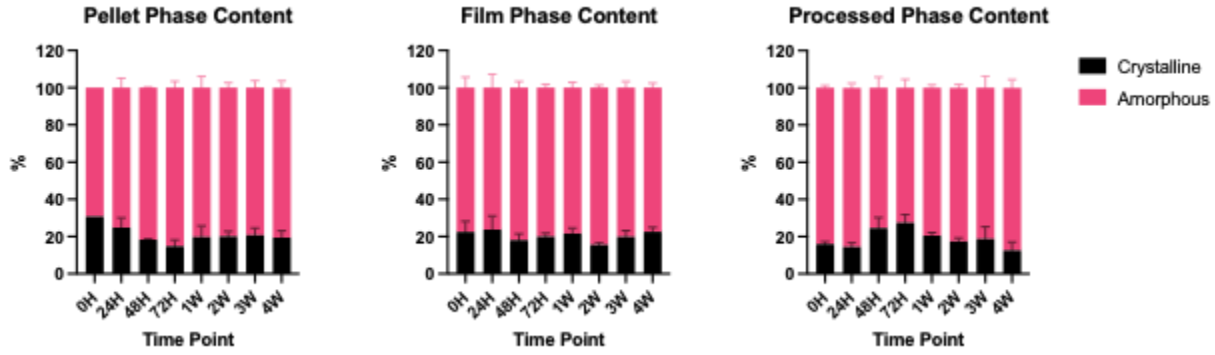

Supplementary Figure 21: Graphs showing phase content of degraded PLGA samples. Only crystallinity and amorphous regions were calculated for these samples.

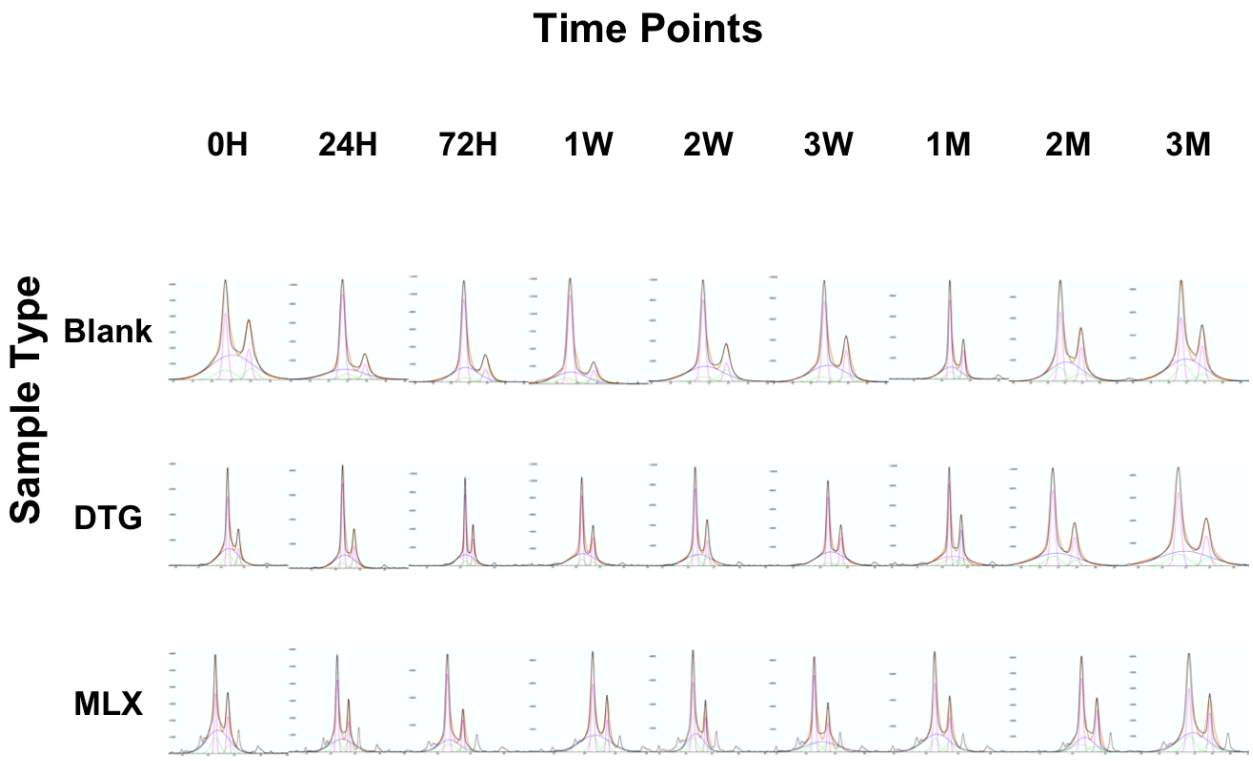

Supplementary Figure 22: Deconvolution comparison of 25℃ PCL implants.

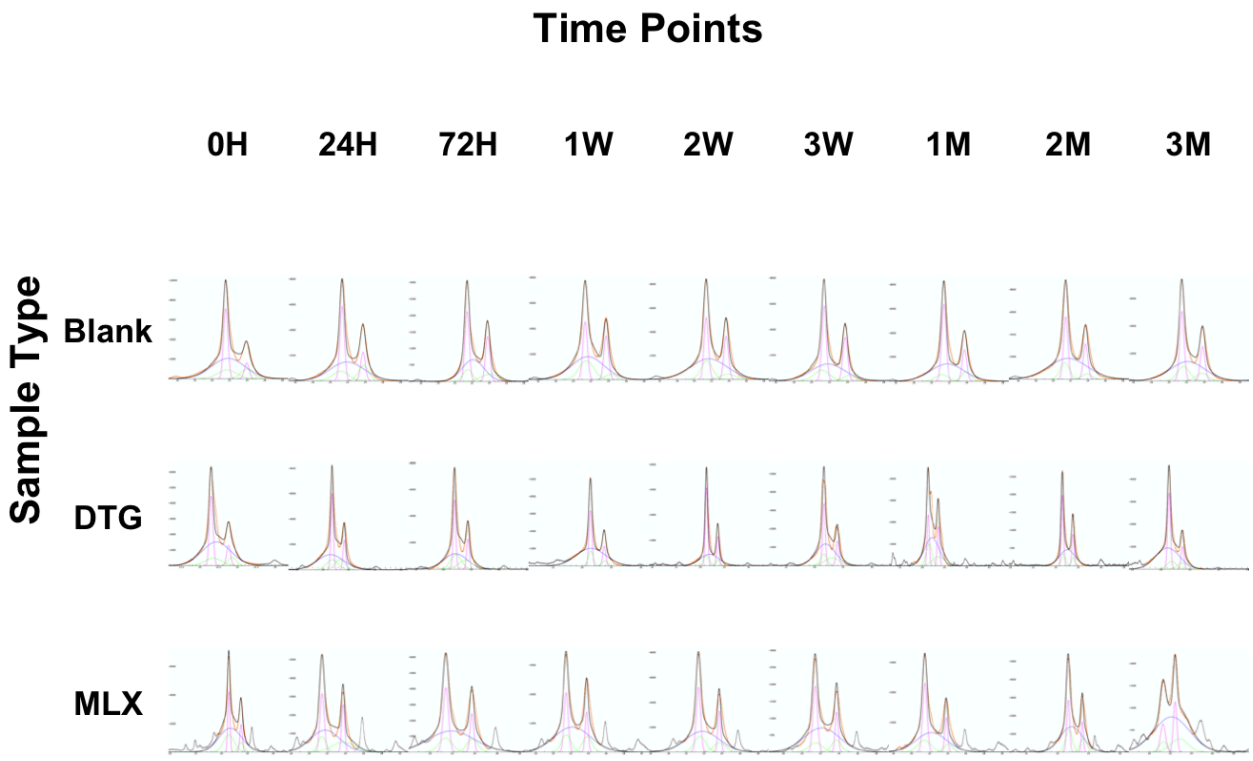

Supplementary Figure 23: Deconvolution comparison of 50℃ PCL implants.